Paleomagnetic study on the Early Permian Gubaoquan doleritic dike swarm in the southern Beishan area, NW China: Implications for the tectonic and paleogeographic reconstructions of the southern Central Asian Orogenic Belt

Xin Zhu, Yan Chen, Bo Wang, Yunpeng Dong, Stéphane Scaillet, Michel Faure, Xinghua Ni, Florian Duval

Journal Pre-proofs

Paleomagnetic study on the Early Permian Gubaoquan doleritic dike swarm in the southern Beishan area, NW China: Implications for the tectonic and paleogeographic reconstructions of the southern Central Asian Orogenic Belt

Xin Zhu, Yan Chen, Bo Wang, Yunpeng Dong, Stéphane Scaillet, Michel Faure, Xinghua Ni, Florian Duval

PII: S1367-9120(23)00293-6
DOI: https://doi.org/10.1016/j.jseaes.2023.105832
Reference: JAES 105832

To appear in: *Journal of Asian Earth Sciences*

Received Date: 16 June 2023
Revised Date: 9 August 2023
Accepted Date: 25 August 2023

Please cite this article as: Zhu, X., Chen, Y., Wang, B., Dong, Y., Scaillet, S., Faure, M., Ni, X., Duval, F., Paleomagnetic study on the Early Permian Gubaoquan doleritic dike swarm in the southern Beishan area, NW China: Implications for the tectonic and paleogeographic reconstructions of the southern Central Asian Orogenic Belt, *Journal of Asian Earth Sciences* (2023), doi: https://doi.org/10.1016/j.jseaes.2023.105832

Paleomagnetic study on the Early Permian Gubaoquan doleritic dike swarm in the southern Beishan area, NW China: Implications for the tectonic and paleogeographic reconstructions of the southern Central Asian Orogenic Belt

Xin Zhu [a, b, c], Yan Chen [c], Bo Wang [b, *], Yunpeng Dong [a], Stéphane Scaillet [c], Michel Faure [c], Xinghua Ni [b, c], Florian Duval [c]

[a] State Key Laboratory of Continental Dynamics, Department of Geology, Northwest University, 710069 Xi'an, China

[b] State Key Laboratory for Mineral Deposits Research, School of Earth Sciences and Engineering, Nanjing University, 210023 Nanjing, China

[c] Institut des Sciences de la Terre d'Orléans, Université d'Orléans, CNRS/INSU, 45071 Orléans, France

[*] Corresponding author: Bo Wang (bwang@nju.edu.cn)

Abstract

To provide further constraints on the tectonic transition and paleogeography of the southern Central Asian Orogenic Belt (CAOB) during the late Paleozoic to early Mesozoic, a paleomagnetic study has been conducted on the Early Permian Gubaoquan doleritic dike swarm in the Beishan region, NW China. Rock magnetic analyses coupled with scanning electron microscope observation show that titanium-poor magnetite is the main magnetic remanence carrier without obvious alteration. Plagioclase $^{40}Ar/^{39}Ar$ dating results reveal that the doleritic dike swarm intruded at ~282-286 Ma, having undergone no intense posterior thermal overprint. Characteristic remanent magnetizations with single reverse polarity are isolated, constituting eight independent directional groups. The isolated remanence is suggested to be primary and averages out the paleosecular variation based on several lines of evidence. Hereby, an Early Permian paleomagnetic pole for the Beishan region is calculated at 82.8°N, 285.6°E, A_{95} = 9.2° with N = 8 direction groups. This new pole fills spatially the Early Permian paleomagnetic data gap in the southern CAOB. The comparison with published contemporaneous paleomagnetic poles in the southern CAOB indicates that 1) the Early Permian paleomagnetic poles of the Beishan region and Dunhuang Block are indistinguishable, indicating insignificant relative movement since then, negating a broad Early Permian ocean between them; 2) the southern CAOB presented a WNW-ESE distributed paleogeography with either a residual ocean or a rift basin in its eastern part in the Early Permian; 3) large-magnitude strike-slip displacements have played a key role in the tectonic activity of the southern CAOB since the Early Permian.

Key Words

Central Asian Orogenic Belt; Paleo-Asian Ocean; Beishan region; Early Permian; Paleomagnetism; Plagioclase $^{40}Ar/^{39}Ar$ dating

1. Introduction

The Central Asian Orogenic Belt (CAOB; Jahn, 2004), approximately equivalent to the Altaïds (Şengör et al., 1993), is the largest Phanerozoic accretionary orogenic belt in the world. It experienced an important transition from collision/accretion to intracontinental tectonics during the late Paleozoic to early Mesozoic (e.g., Eizenhöfer and Zhao, 2018; Han and Zhao, 2018; Wang et al., 2018, 2022; Liu et al., 2019a, b), which is a turning point for understanding the tectonic and paleogeographic evolution of the CAOB (e.g., Wang et al., 2007; Ren et al., 2020; Zhao et al., 2020; Zhang et al., 2021a, b). A better understanding of this transition may shed light on several fundamental problems, such as the geodynamics of intracontinental mega-shear zones, their role in the emplacement of syn-kinematic plutons and pull-apart basins opening (e.g., Wang et al., 2009, 2014; Branquet et al., 2012), stress partitioning and strain localization in regional-scale transpressional and transtensional deformation zones.

Bearing such great significance, the precise time for this tectonic transition, or saying the final closure of the Paleo-Asian Ocean (PAO), remains contentious, albeit numerous studies have been recently carried out (e.g., Xiao et al., 2003, 2010; Han et al., 2011; Xu et al., 2013; Klemd et al., 2015; Eizenhöfer and Zhao, 2018; Loury et al., 2018a). The Beishan region is located between the South Tianshan Suture to the west and the Solonker Fault to the east (Fig. 1a), and thus plays a key role in addressing this problem. The final closure time of the PAO in the Beishan region differs among researchers. Some suggest a post-orogenic extension or a mantle plume setting for the Beishan region in the Early Permian (P_1), indicating that this segment of the PAO closed in the Carboniferous or even earlier (Zhang et al., 2010, 2012; Li et al., 2013; Su et al., 2013; Xu et al., 2021); while others invoke a subduction-related environment during the P_1, implying the existence of a "Liuyuan Ocean" until the Late Permian to Early Triassic (Xiao et al., 2010; Ao et al., 2010; Guo et al., 2012; Mao et al., 2012; Tian and Xiao, 2020). The controversy derives partially from the limited scope of previous approaches, leading to ambiguous tectonic interpretations. Hence, more data are needed to provide constraints to this question from different perspectives (e.g., Chen et al., 2016; Wang et al., 2016; Liu et al., 2019a; Niu et al., 2020). Paleomagnetism is one of the pertinent methods to unravel such puzzles. However, paleomagnetic data in the Beishan region are scarce and mainly focus on Early Paleozoic kinematics and paleogeography (e.g., Huang et al., 2002). Dong et al. (1995) reported preliminary Late Paleozoic paleomagnetic poles for the Beishan region which sheds light on regional tectonic evolution, but this work lacks robust remanence stability tests and the data amount does not meet the current standard.

Moreover, the well-constrained late Paleozoic to early Mesozoic time slices of the southern CAOB, especially the P_1 one, are of great importance to comprehending the process and mechanism of the aforesaid transition. Xiao et al. (2015) and Zhao et al. (2018) put forward Permian paleogeographic reconstructions of the CAOB based

mainly on geologic and paleontologic evidence, prompting a similar scissor-like closure of the PAO with differences in timing. East Asian blocks were paleomagnetically reconstructed in a global frame by Huang et al. (2018) and Dong et al. (2021), whereas some details are worth being refined concerning the P_1 paleogeography of the southern CAOB. Firstly, microcontinents in the southwestern CAOB with high-quality paleomagnetic data, such as the Yili and Turpan-Hami blocks (Zhu et al., 2018, 2019), should be integrated. Secondly, recently published data for the Mongolia Block and North China Craton in the southeastern CAOB (e.g., Zhao et al., 2020; Zhang et al., 2021a) deserve to be incorporated. Thirdly, large-magnitude strike-slip displacements since the late Paleozoic revealed by both geologic and paleomagnetic studies need to be considered (e.g., Laurent-Charvet et al., 2003; Wang et al., 2007; Rolland et al., 2013; He et al., 2021). Most importantly, critically located in the central part of the southern CAOB, the Beishan region currently does not possess any reliable late Paleozoic to early Mesozoic paleomagnetic data, hampering both tectonic and paleogeographic linkages between the southwestern and southeastern parts of the CAOB.

To estimate the scale of the possible P_1 "Liuyuan Ocean" and further constrain the final closure time of the PAO in the Beishan area, a paleomagnetic study has been conducted on the P_1 doleritic dike swarm in the Gubaoquan area along the southern boundary of the CAOB (Fig. 1b-c). The obtained first P_1 Beishan paleomagnetic pole bridges the current data gap across the southern CAOB, making it possible to achieve a well paleomagnetically constrained P_1 paleogeographic reconstruction for the southern CAOB.

2. Geological background and sampling

The CAOB is situated between the Tarim and North China cratons to the south and the Siberia craton to the north (Fig. 1a), being made up of two first-order tectonic units, i.e., the Kazakhstan Orocline and the Tuva-Mongolia Orocline (Şengör et al., 1993; Jahn, 2004; Xiao et al., 2015). As a result of the closure of the PAO, the CAOB was finally amalgamated via the collision alongside its southern margin (Han and Zhao, 2018). Presently, no consensus is achieved concerning the final closure time of the PAO with three major viewpoints: (1) a scissor-like closure from west to east from the Late Carboniferous to the Early Triassic (e.g., Eizenhöfer and Zhao, 2018; Han and Zhao., 2018; Zhao et al., 2018; Liu et al., 2019a, b); (2) a later scissor-like closure from the end of Permian to Middle-Late Triassic (e.g., Zhang et al., 2007; Xiao et al., 2015; Song et al., 2021); and (3) a complex diachronous closure starting from the Devonian (e.g., Xu et al., 2013; Zhao et al., 2013).

The Beishan region is located in the southern margin of the CAOB, connecting the Solonker Fault to the east and the South Tianshan Suture to the west (Fig. 1a; Xiao et al., 2010; Zhang et al., 2015). It truncates the Chinese Eastern Tianshan by the

Xingxingxia Fault to the northwest and is framed by the Dunhuang Block to the south with its eastern part covered by the Badain Jaran Desert (Fig. 1b). From south to north, the Beishan region consists of the Shibanshan, Shuangyingshan, Mazongshan, Hanshan, and Queershan terranes (the latter two are a possible extension of the Eastern Tianshan; e.g., Su et al., 2013; Han and Zhao, 2018); these terranes are separated by the Liuyuan unit, and Hongliuhe-Xichangjing, Jijitaizi-Xiaohuangshan, and Hongshishan ophiolitic mélanges with different ages (Fig. 1b; Xiao et al., 2010; He et al., 2018a).

The Shuangyingshan terrane contains Paleozoic granitic and mafic-ultramafic intrusions, volcanic rocks, and carbonate and clastic rocks. Granitic rocks with different geochemical characteristics intruded between 442 to 217 Ma (He et al., 2018a; references therein). The mafic-ultramafic rocks are interpreted to be emplaced during extensional tectonics between 295 and 260 Ma (e.g., Su et al., 2010, 2013; Xu et al., 2021); however, some other studies indicate for them a subduction-related setting (e.g., Ao et al., 2010; Mao et al., 2012). The 451-367 Ma volcanic rocks are proposed to have formed in a magmatic arc setting (Guo et al., 2014). Carboniferous clastic and carbonate strata are widespread in the western part of the Shuangyingshan terrane, while sparsely exposed among Paleozoic granites in other areas. Permian clastic and volcanic rocks with a pervasively developed sub-vertical cleavage are mainly distributed on the southern part of this terrane (Niu et al., 2020). In the southernmost part of this terrane, medium- to high-grade metamorphic rocks crop out along a 10-km-wide belt in the Gubaoquan area, mainly including gneisses, enclosing retrogressed Ordovician eclogite boudins, quartz schists, and migmatites (He et al., 2018a). To the south, the nearly E-W striking Liuyuan Unit mainly contains Permian basalts (some with a pillow shape), diabases, gabbros, and ultramafic rocks (Mao et al., 2012). Recently, Chen et al. (2016) reported peperites, pillow basalts with interstitial limestones, and thinly-interbedded basalts and limestones from the lower Permian volcano-sedimentary sequence in the Liuyuan area.

Doleritic dikes with NE-SW (40°–60°) strike and vertical to subvertical dip are well developed in the Gubaoquan area, intruding Precambrian gneisses and Silurian-Devonian granites; the emplacement age of the dikes was estimated at 282 ± 6 Ma and 281 ± 4 Ma based on youngest zircons (Zhang et al., 2015; Xu et al., 2021). Their geochemical characteristics reflect an extensional setting although slab break-off and lithosphere delamination scenarios were proposed respectively (Zhang et al., 2015; Xu et al., 2021). Our sampling section is close to the location where the Gubaoquan eclogites were found (Mei et al., 1999; Liu et al., 2011). In this area (N40°59′21″, E95°02′10″ - N40°59′37″, E95°02′24″), numerous vertical to sub-vertical fresh doleritic dikes striking NE-SW intrude Neoproterozoic orthogneisses (Yuan et al., 2015; Fig. 2a-d). Baked contact can be observed between the doleritic dikes and the augen orthogneissic country rock (Fig. 2c-e). Due to poor road conditions, a special sampling strategy was applied in this study. One hundred and twenty-five specimens

were drilled from 20 dikes and their country rock with a portable gasoline drill (section A: BS30; section B: BS31; Fig. 1c). Specifically, six to fifteen specimens were collected from 11 dikes with widths ranging from 3 to 10 m. For the other 9 thinner dikes, two or three specimens were taken from each dike to serve as a qualitative reference group. Sixteen specimens were drilled from 4 sites in the augen gneisses for a possible baked-contact test. For example, orthogneissic specimens were taken from site OG04, located 50 cm, 2 m, and 3 m away from the dike DD05. All specimens were oriented by both magnetic and solar compasses when possible. The average difference between the two azimuth readings was calculated at -2.6° ± 0.6° (1σ), which is used to correct the orientation of samples measured only by a magnetic compass.

3. Methods

Core samples were first cut into standard cylindrical paleomagnetic specimens, i.e. 2.5 cm in diameter and 2.2 cm in length, for the measurements of magnetic remanence and Anisotropy of Magnetic Susceptibility (AMS).

3.1. Rock magnetism and AMS analysis

For revealing the main magnetic minerals of the paleomagnetic samples collected from the doleritic dikes and the orthogneissic country rock, several magnetic experiments were carried out. Thermomagnetic experiments were performed on 5 representative rock powder samples in the atmosphere using a MFK1 susceptibility meter coupled with a CS-4 furnace at the Paleomagnetism Laboratory of the Institut des Sciences de la Terre d'Orléans (ISTO), Orléans University. Three or four cycles of successive heating and cooling to different temperatures were conducted on each sample to better characterize possible mineral transition temperatures during the experiment. Magnetic hysteresis loops of 16 representative samples, using either rock powder or chips, were acquired via a MicroMag Princeton Measurements vibrating sample magnetometer (VSM) equipped in the Paleomagnetism Laboratory of Institut de Physique du Globe de Paris (IPGP). To study the magnetic fabrics, the AMS of specimens were measured using a MFK1 susceptibility meter in the Paleomagnetism Laboratory of the ISTO, Orléans University.

3.2. Scanning electronic microscope (SEM) observation

To visually characterize the main magnetic carrier(s), six representative samples were chosen to make thin sections for SEM observation. This observation was conducted using a Merlin Compact ZEISS SEM coupled with a Bruker (QUANTAX-XFlash6-30mm^2-resolution 129eV) energy dispersive spectroscopy (EDS) system at ISTO, Orléans University. Backscattered SEM images combining the EDS system were used to identify the magnetic minerals. A 15-kV accelerating voltage was set for the instrument during our analysis.

3.3. Plagioclase $^{40}Ar/^{39}Ar$ geochronology

To identify whether the dikes have experienced posterior tectono-thermal event(s), microscopic observations were performed on sample BS30-32, and $^{40}Ar/^{39}Ar$ dating experiments were conducted at the dating laboratory of the ISTO (Orléans University) on the plagioclase selected from doleritic sample BS30-32 using standard selection criteria for freshness. Standard processes (crushing, hand-picking under a binocular microscope, and ultrasonic cleaning) were applied to achieve the highest possible purity of plagioclase concentrates. After neutron irradiation for 10 h in the CLICIT Cd-lined slot of Corvallis Nuclear Reactor (Oregon State University, United States) along with the FCS standard (28.02 ± 0.28 Ma, Renne et al., 1998), $^{40}Ar/^{39}Ar$ experiments were performed on small-sized plagioclase concentrates (N216: 4 grains, 220 µg; N218, 4 grains, 210 µg; N219: 5 grains, 260 µg) using a high-resolution Helix SFT mass-spectrometer outfitted to a home-built CO_2-laser based extraction system featuring ultra-low argon blanks. Detailed operating conditions can be found in Corti et al. (2019). Ages and isotope ratios are plotted and tabulated at ± 2σ and were calculated according to Scaillet (2000). WMA refers to the Weighted Mean Age calculated by inverse-variance weighing of the steps pooled in the weighted mean (as indicated by the arrows in the plots). TGA is Total-Gas Age calculated by summing all the fractions released and by quadratically propagating the attached errors. Pooled age errors include procedural errors, decay constants, and isotope abundance errors.

3.4. Paleomagnetism

Both progressive alternating field (AF) and thermal demagnetizations were used to demagnetize the magnetic remanence. The AF demagnetization was conducted on 45% of specimens through 11-13 steps up to 100 mT with intervals varying from 1 to 20 mT. Around 11-13 steps with a 50°C increment from room temperature to 500°C and a 20-30°C increment from 500°C to 570°C were applied for thermal demagnetization on 55% of specimens. Thermal and AF demagnetizations were carried out using a laboratory-built furnace and a LDA-3 demagnetizer at the Paleomagnetism Laboratories of ISTO, Orléans University. The magnetic remanence of specimens was measured with a JR-5A spinner magnetometer. Demagnetization results were plotted on orthogonal vector diagrams (Zijderveld, 1967). Visually identified linear trajectories were used to isolate characteristic remanent magnetizations and determine directions of magnetic components by principal component analysis, employing a least-square fit comprising three or more demagnetization steps (Kirschvink, 1980), anchoring the fitting lines to the origin where appropriate. Dike-mean directions were computed using the principal component analysis-calculated sample directions with Fisher spherical statistics (Fisher, 1953). The paleomagnetic data were analyzed with PaleoMac software packages offered by Cogné (2003), PMGSC (version 42 by R. Enkin, unpublished), and Paleomagnetism.org (Koymans et al., 2016). Plate reconstructions were built using the open-source software GPlates (*www.gplates.org*).

4. Results

4.1. Rock magnetism and AMS analysis

Thermomagnetic experiments with cycles of successive heating and cooling to different temperatures show obvious increases of magnetic susceptibility during heating at 120-280 ℃ and 400-560 ℃ (Fig. 3a-c), significant decreases at 280-400 ℃ and a sharp one at 560-590 ℃ (Fig. 3a-c), and occasionally tiny decreases at 590-700 ℃ (Fig. 3b-c); much higher magnetic susceptibility is often observed on cooling curves than heating ones (Fig. 3a, 3c). After the paramagnetic correction using the automatic linear function, room-temperature hysteresis loops for most doleritic samples show relatively low coercivity and remanence coercivity (Fig. 3d-e). Loops of other doleritic and all orthogneissic samples indicate soft-coercivity magnetic mineral(s) (Fig. 3f-g). More thermomagnetic experiments and hysteresis loops are shown in Fig. S1.

Accordingly, magnetite is likely the principal magnetic mineral in these rocks with some pyrrhotite and hematite. Multi-phase mineral transitions occurred during heating and cooling, including pyrite altering to magnetite and/or pyrrhotite. After plotting hysteresis parameters of 16 samples from dikes and country rock on the Day plot (Dunlop, 2002), data lie in the region with mixtures of single-domain (SD) and multi-domain (MD) magnetite, and that of dikes is closer to the SD and pseudo-single-domain (PSD) regions (Fig. 3h).

AMS data from the doleritic specimens present a low anisotropy degree (P_J < 1.056) and a slightly prevailing oblate shape (shape parameter T > 0) (Fig. 3i). The K_3 axes (the minimum axis of the magnetic anisotropy ellipsoid; pole of magnetic foliation) are nearly vertical. Most K_1 axes (the maximum axis of the ellipsoid used to represent the magnetic anisotropy; magnetic lineation) are sub-horizontal with a significant convergence in NNE-SSW direction, being nearly parallel to the dikes' strikes (Fig. 3j). The magnetic fabrics of the orthogneissic country rock are scattered (Fig. 3k) and distinct from those of the doleritic dikes.

4.2. SEM observations

Irregular titanium-poor magnetite grains with diameters of 30-150 μm show clear high-temperature exsolution and no evident alteration (Fig. 4a-c). Some titanium-poor magnetite grains with diameters of 50-200 μm also exhibit exsolution, having the appearance of alteration which is probably due to excessive polishing (Fig. 4d). Exsolution dramatically decreases effective grain size and has a profound influence on minerals' magnetic properties (Lindsley, 1976a; 1976b). In our case, a portion of PSD and possible SD (cannot be observed under SEM) magnetite grains could form by this pattern. Abundant irregular pyrite grains and minor ilmenite and chalcopyrite grains are found (Fig. 4e-f). Pyrite grains occasionally show iron oxide rims (Fig. 4g-h). No authigenic magnetic mineral is present within fractures and pores (Fig. 4h-i).

Furthermore, typical pyrrhotite or hematite grain is not observed, possibly due to their low contents and/or small sizes. Corresponding energy-dispersive X-ray spectrometer data are presented in Figs. 4 and S2.

4.3. Plagioclase $^{40}Ar/^{39}Ar$ geochronology

The Gubaoquan dike is mainly composed of plagioclase and pyroxene with similar sizes as well as minor hornblende and Fe-Ti oxides (Fig. 5a-b). The plagioclase is more euhedral than the pyroxene that normally fills in the gaps of intersecting plagioclase crystals, constituting a typical ophitic structure (Fig. 5a-b). The sample BS30-32 is relatively fresh with weak sericitization and chloritization; no obvious recrystallization feature of minerals can be observed (Fig. 5a-b).

Three $^{40}Ar/^{39}Ar$ dating runs were performed on plagioclase extracted from Sample BS30-32 collected on the margin of a 10 m-wide doleritic dike (Figs. 5c and S3; Table S1). Run N216 shows a quasi-plateau age of 283.8 ± 1.8 Ma over the last eleven steps (70% ^{39}Ar released) after some irregular initial steps (Fig. 5c). In contrast, runs N218 and N219 exhibit initial concordant ages of 259.9 ± 2.6 and 265.6 ± 3.0 Ma, respectively, at low temperature (79% and 67% ^{39}Ar released), followed by a common older age over the last steps (16% and 33% ^{39}Ar released, Fig. 5c).

4.4. Paleomagnetism

One hundred and nineteen specimens were paleomagnetically treated using either alternating field (AF) or thermal demagnetization. Low-coercivity and low unblocking temperature component could be identified from 35 specimens by ~10-25 mT or ~200-250 °C in demagnetization (Fig. 6a-b), directing north with downward moderate-deep inclination (D_g = 354.6°, I_g = 58.4°, α_{95} = 5.7°, n = 35). This component is indistinguishable from the present geomagnetic field (D = 0.3°, I = 61.6°; Fig. 6c; Thébault et al., 2015) and is interpreted as a viscous remanent magnetization of the present-day geomagnetic field.

Most AF demagnetized specimens show a high-coercivity (up to 45-70 mT) characteristic remanent magnetization (ChRM) component that trends directly to the origin (Fig. 6d-e). However, a few AF demagnetized specimens show a stable remanent component that trends to the origin over a range of moderate fields, but deviates from the origin at high-field steps (normally >60 mT; Fig. 6f). We consider the component isolated over a range of middle-field steps as ChRM and the high-field component as a mixture of ChRM and secondary remanence carried by high-coercivity phases such as the iron oxide rims of pyrite grains (Fig. 4g-h). In thermal demagnetization, some specimens show a remanence that tends to linearly decay to the origin after removing a low-temperature component (Fig. 6g-h). The remanent directions of most specimens behave erratically after 560 ℃ (Fig. 6h-i), which probably results from abundant newly-formed magnetite during heating (Fig. 3a, 3c). Therefore, comparisons were made

between AF and thermal demagnetization results to obtain representative ChRM directions. Unfortunately, most orthogneissic specimens show chaotic demagnetization behavior (Fig. 6j), and only 3 meaningful ChRMs were isolated from country rock adjacent to the dikes (Figs. 6k and S4; Table 1). The obtained 3 ChRMs share similar directions with the ChRMs isolated from doleritic dikes (Fig. S5), probably reflecting a baked effect. More meaningful ChRMs from country rock samples, especially farther ones (> 2 m away from dikes), are needed to constitute a rigorous baked-contact test.

The dike-mean direction was calculated for each dike, while Fisher statistics were not given for dikes carrying only 2 ChRMs (Table 1). The paleomagnetic results were divided into two groups: Group A contains thick dikes whose mean directions were calculated from at least 5 ChRMs, and their radii of 95 percent probability cone for the mean-direction (α_{95}) range from 1.9° to 8.1°; Group B is composed of qualitative reference dikes with only two or three ChRMs (Table 1). Because no ChRM was isolated from dike DD12, the mean direction of Group A was acquired as D_g = 177.4°, I_g = -51.6°, α_{95} = 7.0°, n = 10 on dike-level (Fig. 7a) and D_g = 178.0°, I_g = -52.0°, α_{95} = 2.5°, n = 67 on specimen-level (Fig. 7b). Group B consists of the remaining 9 dikes with fewer ChRMs and larger α_{95}, and its mean direction was calculated on specimen-level as D_g = 174.0°, I_g = -53.1°, α_{95} = 4.0°, and n = 21 (Fig. 7c).

5. Discussions

5.1. Remanence age and acquisition of the paleomagnetic pole

The $^{40}Ar/^{39}Ar$ run N216 yields a quasi-plateau age of 283.8 ± 1.8 Ma, being consistent with the interpreted U/Pb zircon intrusion age of the Gubaoquan doleritic dikes (Zhang et al, 2015; Xu et al., 2021). The runs N218 and N219 show younger plateau ages at ~260-266 Ma, which reflects either later magma-thermal activity with local ^{40}Ar remobilization because magmatism of such age has been reported in the Beishan area (e.g. in the Xuanwoling and Xijianquanzi areas; Su et al., 2010; Zhang et al., 2010) and Middle Permian strike-slip activities has been widely recognized along the southern rim of the CAOB (e.g., Laurent-Charvet et al., 2003; Loury et al., 2018b), or differential cooling of the plagioclases due to subgrain domain behavior. In either case, a P_1 age can be considered as the time *t* when the dikes cooled over the blocking temperature of titanium-poor magnetite (>500 °C, Fig. 3a-c). Furthermore, based on the weak interaction between the dikes and country rock indicated by the AMS pattern (Fig. 3j-k), we suggest that the second scenario is unlikely, and thus *t* should be ~282-286 Ma.

The isolated ChRMs from the doleritic specimens are interpreted to be primary based on the following arguments. Abundant titanium-poor magnetite grains with diameters of 30-200 μm are observed under SEM, showing irregular shapes and no intense alteration (Fig. 4a-d). The clear high-temperature exsolution decreases effective grain size, reasonably having formed smaller PSD and SD grains that are stable carriers

of primary remanence (Fig. 4a-d; Butler, 1992). No authigenic mineral within fractures and pores is found under SEM, precluding any chemical remagnetization resulting from orogenic fluids (Fig. 4h-i; Jiao et al., 2019; Zhang et al., 2019). The possible weak influence of posterior magma-thermal events, which only partially reset the $^{40}Ar/^{39}Ar$ system of plagioclase (225–300 °C; Cassata et al., 2009) at 266-260 Ma, is unable to blur the P_1 ChRMs carried by magnetite, excluding intense thermal remagnetization. Although more data are needed to constitute a more rigorous baked-contact test, the available results from country rocks probably indicate a baked effect produced by the intrusion of doleritic dikes (Fig. S5). In addition, the doleritic samples' hysteresis parameters distribute in the SD-MD mixing region, which is supposed to be a hint of primary remanence (Huang et al., 2017; Fig. 3h). Furthermore, the low P_J value of the doleritic dikes suggests no intense posterior deformation (Fig. 3i).

No overlying stratum is preserved, disabling a direct tilt correction derived from the attitude of cover rocks. In addition, the Permian strata outcropped near and in the southeast of the Gubaoquan-Hongliuyuan fault are thought to be inappropriate to perform a tilt correction on the studied doleritic dikes because these strata with pervasive cleavage could have experienced a different tectonic evolution from that of the doleritic dikes. Moreover, the strata near and in the southeast of the Gubaoquan-Liuyuan fault show generally ENE-WSW strike, and their dip angles increase from 9° at 20 km southward apart from the fault to 83° alongside the fault (GBGP, 1967), resembling an attitude pattern caused by strike-slip displacement rather than N-S convergence.

Given this, the AMS results serve as the only available data to estimate the potential tilting so far. Because the doleritic dike samples generally show an insignificant Hopkinson effect (Figs. 3a-c and S1), we interpret that the PSD magnetite is probably dominant carrying a normal magnetic fabric. The AMS pattern of the studied dikes is rather interesting, yet difficult to understand. It exhibits a principal NNE-SSW k_1 direction with a vertical K_3 direction, resembling a sedimentary fabric (Fig. 3j). This magnetic fabric could be interpreted by the following acquisition mechanism: the doleritic magma ascended vertically, but when it cooled down with sufficient crystals its viscosity increased significantly. The balance between gravity and buoyancy coupled with pressure could not support vertical flow, then subhorizontal flow with pushes of newly coming magma was possible, and the AMS was probably obtained and recorded during the last stage. Taking into consideration this AMS acquisition mechanism and the vertical to sub-vertical geometry of the doleritic dikes (Fig. 2), the studied dikes have probably undergone insignificant tilting. On these premises, all doleritic rocks hold a sole reversed polarity, which is consistent with remanence acquisition during the Kiaman Reverse Superchron (Opdyke & Channell, 1996), supplementing an argument for primary remanence.

Paleosecular variation (PSV) has to be averaged out before discussing any tectonic

implication because paleomagnetic data from a single dike are regarded as a spot reading of the geomagnetic field (Lippert et al., 2014). Only dike-mean directions from Group A are chosen to evaluate directional independence using a common direction test (McFadden and McElhinny, 1990). Doleritic dikes DD09 and DD10, as well as DD13 and DD14, share identical directions, respectively, and thus they are grouped as DDs0910 and DDs1314 (Fig. 8a). Consequently, the mean direction of the 8 direction groups is calculated as D_g = 177.9°, I_g = -52.7°, α_{95} = 7.8°, n = 8 (Fig. 8a), and a Fisher mean virtual geomagnetic pole (VGP) is derived from 8 corresponding VGPs at 82.8°N, 285.6°E with A_{95} = 9.2° (A_{95}, the radius of the circle of 95% confidence about the pole; Fig. 8b). The angular dispersion (S = 13.3°) of our data is comparable to that observed in VGP populations from 0 to 5 Ma lavas at similar latitudes (paleolatitude λ = 33.9° ± 9.2°; $S_{\lambda 28.6}$ = 15.6° [12.5°, 18.8°], $S_{\lambda 36.1}$ = 15.7° [14.4°, 17.0°]; Johnson et al., 2008). The A_{95} (2.85°) of our ChRMs is within the *N*-dependent A_{95} envelope (A_{95min} = 2.23, A_{95min} = 5.80) proposed by Deenen et al. (2011). These results suggest that the PSV appears to have been averaged out, though the number of valid dikes is relatively limited. In addition, the mean directions on specimen-level of Group A and Group B are indistinguishable with an angular difference of 2.7° ± 4.7° (Fig. 8c), suggesting that more sampling would yield essentially a coherent result with a smaller confidence interval. In summary, the Fisher mean VGP (82.8°N, 285.6°E with A_{95} = 9.2°) can be considered as the P_1 (at ~282-286 Ma) paleomagnetic pole for the Beishan region.

5.2. The scale of the P_1 Liuyuan Basin & the final closure time of the middle segment of the PAO

We would like to acknowledge that two inadequacies exist in our study which are indirect structural control and lack of robust remanence stability tests. No suitable stratum could be found to perform an adequate structural control on the original occurrence of the studied doleritic dikes, and the AMS results serve as the only constraint. Most remanence stability tests cannot be applied in our case because the studied dikes intruded during the Kiaman Reverse Superchron for the reversal test and are short of structural control for the fold one. The baked-contact test seems to be feasible. Unfortunately, only 3 ChRMs out of 16 specimens were obtained from country rocks due to their weak remanent magnetization, though reflecting a baked effect, being unable to constitute a positive test. However, as discussed above, several lines of evidence argue that the ChRMs isolated from the dikes are primary. These two inadequacies cannot be perfectly solved so far, therefore, they should be kept in mind when discussing the implications of our newly obtained paleomagnetic pole.

Xu et al. (2019) reported the first P_1 paleomagnetic pole for the Dunhuang Block with high-quality geochronologic constraints, passing both fold and reverse tests, suggesting no significant inclination shallowing (Fig. 9a; Table S2). A quite small A_{95} (1.6°) was obtained for this pole, whereas the samples contain mainly sandstones and sedimentary tuffs. As the Dunhuang Block and the Beishan region are separated by the

Liuyuan Unit considered as a suture zone, these poles constitute a key coeval pair to permit an estimation of the possible existence of an oceanic basin between them at the P_1 time. The angular difference between the P_1 paleomagnetic poles of the Beishan region (~282-286 Ma) and Dunhuang Block (281-291 Ma; Xu et al., 2019) is calculated as 8.9° ± 9.3° (reference point: 41°N, 95°E), which is paleomagnetically insignificant. Therefore, the Beishan region and Dunhuang Block have been paleomagnetically welded together at least since the P_1, and no broad oceanic basin existed between them in the P_1.

Previous researchers have not reached a consensus on the P_1 tectonic setting of the Liuyuan Basin. Some suggest a subduction-related environment, while others invoke a post-orogenic extension or a mantle plume setting. The debate derived from contrary geologic evidence: (1) P_1 ophiolites (286 ± 2 Ma) in the Liuyuan Unit are reported (Xiao et al., 2010; Mao et al., 2012), whereas peperites and other facies originating from magma-sediment mingling are found from the Lower Permian strata in the Liuyuan and Hongliuhe areas (Chen et al., 2016), and the pillow lavas in the Liuyuan Unit are interlayered with lacustrine sandstone, claystone and clayey lake deposits (Wang et al., 2016); (2) Subduction-related P_1 mafic-ultramafic complexes are reported in the Hongshishan (282 ± 3 Ma) and Pobei areas (Ao et al., 2010), but a post-orogenic extensional setting is suggested for the Bijiashan and other complexes in the Beishan region (Su et al., 2013). Moreover, widespread P_1 alkali-rich high-potassium granites (e.g., Zhang et al., 2012; Li et al., 2013) and bimodal igneous series (e.g., Su et al., 2013; Wang et al., 2016) are recorded in the southern Beishan; (3) A major P_1 tectonic separation is proposed between the Beishan region and Dunhuang Block based on provenance analysis and isotopic characteristics of the sedimentary rocks (Guo et al., 2012; Liu et al., 2019a); however, the detritus from the Dunhuang Block is suggested to arrive in the Beishan region before the Visean (347 - 331 Ma; Niu et al., 2020), and Tian and Xiao (2020) consider rocks cropping out on both sides of the Liuyuan Basin are comparable both in lithology and age. Although the separation and mixture between the Angara flora and the Cathaysia flora would shed light on the late Paleozoic paleogeographic evolution of the southern CAOB (Deng et al., 2009; Ren et al., 2020), available paleontologic data cannot help settle the abovementioned dispute so far.

Based on our new paleomagnetic results, the scale of the P_1 Liuyuan Basin between the Beishan region and Dunhuang Block would not be as considerable as a conventional ocean. Therefore, the Liuyuan Basin was more likely under a post-orogenic extension or a mantle plume setting in the P_1 as the geological facts support. Furthermore, the middle segment of the PAO closed at least in the P_1, appealing for pre-Permian paleomagnetic works to provide key constraints on the final closure time.

5.3 Tectonic implications and P_1 paleogeographic reconstruction of the southern CAOB

The compilation of P_1 paleomagnetic poles for the major blocks in the southern CAOB is shown in Fig. 9a and described in detail in Text S1 and Table S2 (Cheng et al., 1985; Bai et al., 1987; Sharps et al., 1989, 1982; Zhao et al., 1990; Li et al., 1991; Ma et al., 1992; Pruner et al., 1992; Nie et al., 1993; Wu et al., 1993; Li et al., 1995; Fang et al., 1996; Chen et al., 1997; Xu et al., 1997; Huang et al., 1999; Choulet et al., 2011, 2013; Li et al., 2012; Zhao et al., 2013, 2020; Yuan and Yang, 2015a, 2015b; Zhang et al., 2018, 2021a, 2021b; Zhu et al., 2018, 2019; Wei et al., 2020).

From a regional scale, keeping in mind the confidence intervals, it is clear that the P_1 pole of the Beishan region clusters together with the poles of Yili, Turpan-Hami, and Dunhuang blocks (Fig. 9a), suggesting that they have been quasi-amalgamated together at least since the P_1 and no paleomagnetically significant relative movement occurred among them thereafter. In contrast, the P_1 poles of Tarim and Junggar blocks are different from the poles of the above blocks with significant relative rotation and weak latitudinal movement (Fig. 9a). Such movements were previously interpreted as the result of the large-magnitude strike-slip displacements along mega-shear zones and the closure of pull-apart basins triggered by strike-slip displacements since the P_1 (e.g., Wang et al., 2007; Zhu et al., 2018, 2019).

These conclusions are supported by geologic evidence, for instance, the formation of ophiolites in the Tianshan and Beishan regions lasted until the Carboniferous, with no unambiguous Permian ophiolite assemblages (Han and Zhao, 2018; reference therein). The (U)HP complexes mainly exposed in the Akeyazi and Atbashi areas have Pennsylvanian ages of peak metamorphism and exhumation (e.g., Klemd et al., 2005, 2011; Simonov et al., 2008; Loury et al., 2018a). P_1 A-type granitoids are widespread in the western and central southern CAOB, reflecting mantle plume and/or post-collisional extension/strike-slip settings (e.g., Zhang et al., 2010; Dong et al., 2011; Li et al., 2013; Loury et al., 2018b). Large-magnitude intracontinental strike-slip displacements occurred in this region since the P_1 as revealed by both structural and kinematic studies and geochronologic results (e.g., Laurent-Charvet et al, 2003; Loury et al., 2017; He et al., 2018b, 2021; Rolland et al., 2020).

By compiling the available paleomagnetic data from the southern CAOB, the following primary features can be observed (Fig. 9a): there are no obvious latitudinal differences among major blocks either in the western, central, or eastern parts of the southern CAOB since the P_1, respectively; the P_1 paleomagnetic poles of the major blocks in the southern CAOB principally distribute along a small circle fitting at our sampling site, revealing large relative rotations among them since then; the P_1 paleolatitude of the major blocks in the southern CAOB progressively decreases eastward (reference site: 41.0°N, 95.0°E) from 34° ± 6°N (1σ, west), ~30°N (only 2 poles, middle) to ~26° ± 4°N (1σ, east).

Our newly obtained P_1 paleomagnetic pole for the Beishan region bridges the data

gap between the southwestern and southeastern CAOB, providing constraints on the transition from convergent to intracontinental tectonics in the southern CAOB: (1) No broad ocean basin existed in the southern CAOB during the P_1. As indicated by paleomagnetic and geologic evidence above, the west and central segments of the PAO probably closed at least in the P_1. Further east, a residual ocean basin with < 580 ± 790 km width likely existed between the Xilinhot-Songliao Block and North China Craton at ~265 Ma (Ren et al., 2020). Terrestrial floras were different on either side of the Solonker Suture during the Middle Permian (temperate Angara flora to the north and tropical-subtropical Cathaysia flora to the south), whereas marine fauna like Zhesi brachiopods was free to mingle then, supporting a small ocean basin (Shen and Shi, 2002; Deng et al., 2009). The nature of this Permian ocean basin (long-lived or reopened) remains unclear (e.g., Xiao et al., 2003; Xu et al., 2013; Eizenhöfer and Zhao, 2018; Ren et al., 2020; Zhao et al., 2020); (2) Large-magnitude intracontinental strike-slip displacements and related local vertical-axis rotations acted as the major tectonic pattern since the P_1 in the southern CAOB. In addition to the shearing up to several hundred kilometers along the Erqishi, North Tianshan, and Nalati Faults (Wang et al., 2007; Zhu et al., 2018, 2019), strike-slip-related rotations are also borne out by Mesozoic shear zones within and along the margin of the Mongolia Block, such as the Xilamulun Fault (Zhao et al., 2015) and East Gobi Fault (Webb et al., 2010). The counterclockwise rotation of the Mongolia Block poles with respect to the North China Craton poles is interpreted by the sinistral shear along the East Gobi Fault Zone (Zhao et al., 2020); (3) Chiefly based on available paleomagnetic data, taking into consideration the large-magnitude strike-slip movements and other geologic and paleontologic evidence, a P_1 paleogeographic reconstruction for the southern CAOB is achieved (Fig. 9b). The major blocks in the southern CAOB presented a WNW-ESE distributed paleogeography in the P_1 with a rift basin or residual ocean basin in the eastern part (Fig. 9b; Huang et al., 2018; Zhao et al., 2020; Ren et al., 2020). Presently, the highest latitude of the southeastern CAOB mainly resulted from the Mesozoic closure of the Mongol-Okhotsk Ocean (Zhao et al., 1990; Zhao et al., 2020).

6. Conclusions

1. New plagioclase $^{40}Ar/^{39}Ar$ geochronological results from the Gubaoquan doleritic dike swarm indicate that the dikes intruded at ~282-286 Ma.

2. Rock magnetic mineralogical study and scanning electron microscope observations reveal a primary magnetic remanence for the Gubaoquan dikes. Hereby, the first Early Permian paleomagnetic pole (~282-286 Ma) for the Beishan region is calculated at 82.8°N, 285.6°E, A_{95} = 9.2°, and N = 8 direction groups.

3. The insignificant polar difference (8.9° ± 9.3°) between Beishan region and Dunhuang Block indicates no obvious relative movement occurred between them since the Early Permian, negating a broad Early Permian ocean between them.

4. The southern CAOB presented a WNW-ESE distributed paleogeography with a rift basin or residual ocean in its eastern part in the Early Permian.

5. Large-magnitude strike-slip displacements have played a key tectonic role in the southern CAOB since the Early Permian.

Data availability

All data related to this work can be found in the manuscript and supplementary materials. Specimen-level paleomagnetic analyses are presented in the Supplementary Material as Table S3.

Acknowledgments

We thank Saloua Ouggahi, Yohan Guyodo, France Lagroix, Gonzalez Cano Adriana, Maria Jiménez Mejías, and Ida Di Carlo for their help in the laboratories. The Editor Prof. Ibrahim Uysal, Prof. Yann Rolland and two anonymous reviewers are appreciated for their constructive comments and suggestions. Prof. Huang B. C. is thanked for his suggestions on the early version of the manuscript. This study was co-sponsored by the National Natural Science Foundation of China (42161144013, 42202234, 41772225) and China Postdoctoral Science Foundation (2021M692606). The Youth Innovation Team of Shaanxi Universities, the MOST Special Fund from the State Key Laboratory of Continental Dynamics, Northwest University, the China Scholarship Council (201806190163), LABEX VOLTAIRE (ANR-10-LABX-100-01), and EQUIPEX PLANEX (ANR-11-EQPX-0036) projects are appreciated.

References

Ao, S. J., Xiao, W. J., Han, C. M., Mao, Q. G., & Zhang, J. E., 2010. Geochronology and geochemistry of Early Permian mafic–ultramafic complexes in the Beishan area, Xinjiang, NW china: Implications for late Paleozoic tectonic evolution of the southern Altaids. *Gondwana Res.* 18(2-3), 466-478. DOI: 10.1016/j.gr.2010.01.004

Bai, Y., Chen, G., Sun, Q., Sun, Y., Li, Y., Dong, Y., Sun, D., 1985. Late Paleozoic polar wander path for the Tarim platform and its tectonic significance. *Tectonophysics* 139(1–2), 145–153. DOI: 10.1016/0040-1951(87)90203-4

Branquet, Y., Gumiaux, C., Sizaret, S., Barbanson, L., Wang, B., Cluzel, D., Li, G. R., Delaunay, A., 2012. Synkinematic mafic/ultramafic sheeted intrusions: Emplacement mechanism and strain restoration of the Permian Huangshan Ni–cu ore belt (eastern Tianshan, NW China). *J. Asian Earth Sci.* 56, 240–257. DOI: 10.1016/j.jseaes.2012.05.021

Butler, R. F., 1992. Paleomagnetism: Magnetic domains to geologic terranes. Boston: Blackwell Scientific Publications.

Cassata W. S., Renne P. R., Shuster D. L., 2009. Argon diffusion in plagioclase and implications for thermochronometry: A case study from the Bushveld Complex, South Africa. *Geochim. Cosmochim. Acta* 73, 6600–6612. DOI: 10.1016/j.gca.2009.07.017

Chen, H., Dobson, J.P., Heller, F., Hao, J., 1997. Preliminary paleomagnetic results from the Upper Carboniferous of Uliastai Block, Inner Mongolia, China. *Geophys. Res. Lett.* 24, 2833-2836. DOI: 10.1029/97GL02897

Chen, S., Guo, Z. J., Qi, J. F., Zhang, Y. Y., Pe-Piper, G. Piper, D. J. W., 2016. Early Permian volcano-sedimentary successions, Beishan, NW China: Peperites demonstrate an evolving rift basin. *J. Volcanol. Geoth. Res.* 309, 31-44. DOI: 10.1016/j.jvolgeores.2015.11.004

Cheng, G. L., Bai, Y. H., Li, Y. A., 1983. Paleomagnetism of Lower Permian in the Wusha-Aksu area of Xinjiang. *Seismol. and Geol.* 5(4), 12-12 (in Chinese).

Choulet, F., Chen, Y., Cogné, J. P., Rabillard, A., Wang, B., Lin, W., Michel, F., Cluzel, D., 2013. First Triassic palaeomagnetic constraints from Junggar (NW China) and their implications for the Mesozoic tectonics in Central Asia. *J. Asian Earth Sci.* 78, 371–394. DOI: 10.1016/j.jseaes.2013.01.023

Choulet, F., Chen, Y., Wang, B., Faure, M., Cluzel, D., Charvet, J., Lin, W., Xu, B., 2011. Late Paleozoic paleogeographic reconstruction of Western Central Asia based upon paleomagnetic data and its geodynamic implications. *J. Asian Earth Sci.* 42(5), 867–884. DOI: 10.1016/j.jseaes.2010.07.011

Cogné, J. P., 2003. PaleoMac: A MacintoshTM application for treating paleomagnetic data and making plate reconstructions. *Geochem. Geophy. Geosy.* 4(1), 1007. DOI: 10.1029/2001GC000227

Corti, G., Cioni, R., Franceschini, Z., Sani, F., Scaillet, S., Glerum, A., 2019. Aborted propagation of the Ethiopian rift caused by linkage with the Kenyan rift. *Nat. commun.* 10, 1309. DOI: 10.1038/s41467-019-09335-2

Deenen, M. H. L., Langereis, C. G., Van Hinsbergen, D. J. J., Biggin, A. J., 2011. Geomagnetic secular variation and the statistics of palaeomagnetic directions. *Geophys. J. Int.* 186(2), 509–520. DOI: 10.1111/j.1365-246X.2011.05050.x

Deng, S., Wan, C., Yang, J., 2009. Discovery of a late Permian Angara-Cathaysia mixed flora from Acheng of Heilongjiang, China, with discussions on the closure of the Paleoasian Ocean. *Sci. China Ser. D Earth Sci.* 52(11), 1746–1755. DOI: 10.1007/s11430-009-0200-2

Dong, X. B., Yang, H. X., Li, P. W., 1995. The Paleomagnetic study of terrane tectonics in geoscience transection from Golmud to Ejin Qi. *Chinese J. Geophys.* 38(1), 71-85. (in Chinese with English abstract) DOI: CNKI:SUN:DQWX.0.1995-S2-007

Dong, Y. P., Sun, S. S., Santosh, M., Zhao, J., Sun, J. P., He, D. F., Shi, X. H., Hui, B., Cheng, C., Zhang, G. W., 2021. Central China Orogenic Belt and amalgamation of East Asian continents. *Gondwana Res.* 100, 131-194. DOI: 10.1016/j.gr.2021.03.006

Dong, Y. P., Zhang, G. W., Neubauer, F., Liu, X. M., Hauzenberger, C., Zhou, D. W., Li, W., 2011. Syn-and post-collisional granitoids in the Central Tianshan orogen: geochemistry, geochronology and implications for tectonic evolution. *Gondwana Res.* 20, 568–581. DOI: 10.1016/j.gr.2011.01.013

Dunlop, D. J., 2002. Theory and application of the Day plot (Mrs/Ms versus Hcr/Hc): 2. Application to data for rocks, sediments, and soils. *J. Geophys. Res.* 107(B3), 2057, DOI: 10.1029/2001JB000487

Eizenhöfer, P. R., Zhao, G. C, 2018. Solonker Suture in East Asia and its bearing on the final closure of the eastern segment of the Palaeo-Asian Ocean. *Earth Sci. Rev.* 186, 153–172. DOI: 10.1016/j.earscirev.2017.09.010

Fang, D. J., Jin, G. H., Jiang, L. P., Wang, P. Y., Wang, Z. L., 1996. Paleozoic paleomagnetic results and the tectonic significance of Tarim plate. *Chinese J. Geophys.* 39(4), 522–532 (in Chinese with English abstract).

Fisher, R. (1953). Dispersion on a sphere. *Proc. R. Soc. London*, 217(1130), 295–305. DOI: 10.1098/ rspa.1953.0064

Guo, Q. Q., Xiao, W. J., Hou, Q. L., Windley, B. F., Han, C. M., Tian, Z. H., Song, D. F., 2014. Construction of Late Devonian Dundunshan arc in the Beishan orogen and its implication for tectonics of southern Central Asian Orogenic Belt. *Lithos*, 184-187, 361-378. DOI: 10.1016/j.lithos.2013.11.007

Guo, Q. Q., Xiao, W. J., Windley, B. F., Mao, Q. G., Han, C. M., Qu, J. F., Ao, S. J., Li, J. L., Song, D. F., Yong, Y., 2012. Provenance and tectonic settings of Permian turbidites from the Beishan mountains, NW China: Implications for the late Paleozoic accretionary tectonics of the southern Altaids. *J. Asian Earth Sci.* 49, 54-68. DOI: 10.1016/j.jseaes.2011.03.013

Han, B. F., He, G. Q., Wang, X. C., Guo, Z. J., 2011. Late carboniferous collision between the Tarim and Kazakhstan–Yili terranes in the western segment of the South Tian Shan Orogen, Central Asia, and implications for the northern Xinjiang, western China. *Earth Sci. Rev.* 109(3-4), 74–93. DOI: 10.1016/j.earscirev.2011.09.001

Han, Y. G. Zhao, G. C., 2018. Final amalgamation of the Tianshan and Junggar orogenic collage in the southwestern Central Asian Orogenic Belt: Constraints on the closure of the Paleo-Asian Ocean. *Earth Sci. Rev.* 186, 129-152. DOI: 10.1016/j.earscirev.2017.09.012

He, Z. Y., Klemd, R., Yan, L. L., Zhang, Z. M., 2018a. The origin and crustal evolution of microcontinents in the Beishan orogen of the southern Central Asian Orogenic Belt. *Earth Sci. Rev.* 185, 1-14. DOI:10.1016/j.earscirev.2018.05.012

He, Z. Y., Wang, B., Zhong, L. L., Zhu, X. Y., 2018b. Crustal evolution of the Central Tianshan Block: Insights from zircon U-Pb isotopic and structural data from meta-sedimentary and meta-igneous rocks along the Wulasitai – Wulanmoren shear zone. *Precambrian Res.* 314, 111-128. DOI: 10.1016/j.precamres.2018.06.003

He, Z. Y., Wang, B., Ni, X H., De Grave, J., Scaillet, S., Chen, Y., Liu, J. S., Zhu, X., 2021. Structural and kinematic evolution of strike-slip shear zones around and in the Central Tianshan: Insights for eastward tectonic wedging in the southwest Central Asian Orogenic Belt. *J. Struct. Geol.* 144, 104279. DOI: 10.1016/j.jsg.2021.104279

Huang, B. C., Otofuji, Y., Yang, Z. Y., 1999. Paleomagnetic constraints on the tectonic relationship between the Alashan/Hexi Corridor Terrane and the North China Block. *Geophys. Res. Lett.* 26(6), 787-790. DOI: 10.1029/1999GL900097

Huang, B. C., Wang, Y. C., Zhu, R. X., Zhang, F, Q., 2002. Paleomagnetism of early Paleozoic volcanic rocks from the Beishan area, Gansu of northwest China: Preliminary insight into early Paleozoic kinemics of the Beishan Terrane. *Chinese Sci. Bull.* 47(18), 1561-1567. DOI: 10.1360/02tb9344

Huang, B. C., Yan, Y. G., Piper, J. D. A., Zhang, D. H., Yi, Z. Y., Yu, S., Zhou, T. H., 2018. Paleomagnetic constraints on the paleogeography of the East Asian blocks during late

Paleozoic and early Mesozoic times. *Earth Sci. Rev.* 8-36. DOI: 10.1016/j. earscirev.2018.02.004

Huang, W., Lippert, P. C., Zhang, Y., Jackson, M. J., Dekkers, M. J., Li, J., Hu, X., Zhang, B., Guo, Z., Van Hinsbergen, D. J. J., 2017. Remagnetization of carbonate rocks in southern Tibet: Perspectives from rock magnetic and petrographic investigations. *J. Geophys. Res*. 122(4), 2434-2456. DOI: 10.1002/2017JB013987

Jahn, B. M., 2004. The Central Asia Orogenic Belt and growth of the continental crust in the Phanerozoic. In J. Malpas et al. (Eds.), Aspects of the tectonic evolution of China. *Geol. Soc. London, Special Pub.* 226, 73–100. DOI: 10.1144/GSL.SP.2004.226.01.05

Johnson, C. L., Constable, C. G., Tauxe, L., Barendregt, R., Brown, L. L., Coe, R. S., Layer, P., Mejia, V., Opdyke, N. D., Singer, B. S., Staudigel, H., Stone, D. B., 2008. Recent investigations of the 0–5 Ma geomagnetic field recorded by lava flows. *Geochem. Geophy. Geosy.* 9, Q04032. DOI: 10.1029/2007GC001696

Jiao, W., Li, Y., Yang, Z., Liu, J., 2019. A widespread Early Mesozoic remagnetization in South China. *J. Geophys. Res.* 124, 88–103. DOI: 10.1029/2018JB016707

Kirschvink, J. L., 1980. The least squares line and the analysis of paleomagnetic data. *Geophy. J. Inter.*, 62(3), 699–718. DOI: 10.1111/j.1365246X.1980.tb02601.x

Klemd, R., Bröcker, M., Hacker, B. R., Gao, J., Gans, P., Wemmer, K., 2005. New age constraints on the metamorphic evolution of the high-pressure/low-temperature belt in the western Tianshan Mountains, NW China. *J. Geol.* 113, 157–168. DOI: 10.1086/427666

Klemd, R., Gao, J., Li, J. L., Meyer, M., 2015. Metamorphic evolution of (ultra)-high-pressure subduction-related transient crust in the South Tianshan Orogen (Central Asian Orogenic Belt): geodynamic implications. *Gondwana Res.* 28, 1–25. DOI: 10.1016/j.gr.2014.11.008

Koymans, M. R., Langereis, C. G., Pastor-Galán, D., Hinsbergen, D. J. J. V., 2016. Paleomagnetism.org: An online multi-platform open source environment for paleomagnetic data analysis. *Compu. & Geosci.*, 93, 127–137. DOI: 10.1016/j.cageo.2016.05.007

Laurent-Charvet, S., Charvet, J., Monié, P., Shu, L. S., 2003. Late Paleozoic strike-slip shear zones in eastern Central Asia (NW China): New structural and geochronological data. *Tectonics*, 22(2), 1009. DOI: 10.1029/2001TC901047

Li, P., Zhang, S., Gao, R., Li, H., Zhao, Q., Li, Q., Guan, Y., 2012. New Upper Carboniferous-Lower Permian Paleomagnetic Results from the Central Inner Mongolia and Their Geological Implications. *J. Jilin Univ.* (Earth Sci. Edition), 42, 423-434 (in Chinese with English abstract). DOI: 10.13278/j.cnki.jjuese.2012.s1.053

Li, S., Wilde, S. A., Wang, T., 2013. Early Permian post-collisional high-k granitoids from Liuyuan area in southern Beishan orogen, NW China: Petrogenesis and tectonic implications. *Lithos*, 179, 99-119. DOI: 10.1016/j.lithos.2013.08.002

Li, Y. A., Li, Q., Zhang, H., Sun, D. J., Cao, Y., Wu, S. Z., 1995. Paleomagnetic study of Tarim and its adjacent area as well as the formation and evolution of the basin. *Xinjiang Geol.* 13(4), 293–378 (in Chinese with English abstract). DOI: CNKI:SUN:XJDI.0.1995-04-000

Li, Y. P., Sharps, R., Mcwilliams, M., Li, Y., Li, Q., Zhang, W., 1991. Late Paleozoic paleomagnetic results from the Junggar block, northwestern China. *J. Geophys. Res.* 96(B10), 16047–16060. DOI: 10.1029/91JB01619

Lindsley, D. H., 1976a. The crystal chemistry and structure of oxide minerals as exemplified by the Fe-Ti oxides, in: Oxide Minerals, ed: D. Rumble, III, Mineralogical Society of America, Washington, D.C., 1–60.

Lindsley, D. H.,1976b. Experimental studies of oxide minerals, in: Oxide Minerals, ed: D. Rumble, III, Mineralogical Society of America, Washington, D.C., 61–88.

Lippert, P. C., Van Hinsbergen, D. J., Dupont-Nivet, G., 2014. Early Cretaceous to present latitude of the central proto-Tibetan Plateau: A paleomagnetic synthesis with implications for Cenozoic tectonics, paleogeography, and climate of Asia. *Geol. Soc. America Special Papers*, 507, 1–21. DOI: 10.1130/2014.2507(01)

Liu, Q., Zhao, G. C., Han, Y. G., Zhu, Y. L., Wang, B., Eizenhöfer, P. R., Zhang, X. R., 2019a. Detrital zircon provenance constraints on the final closure of the middle segment of the Paleo-Asian Ocean. *Gondwana Res.* 69, 73–88. DOI: 10.1016/j.gr.2019.01.001

Liu, Q., Zhao, G.C., Han, Y.G., Zhu, Y.L., Wang, B., Eizenhöfer, P.R., Zhang, X.R., Tsui, R.W.T., 2019b, Timing of the final closure of the middle segment of the Paleo–Asian Ocean: Insights from geochronology and geochemistry of Carboniferous–Triassic volcanosedimentary successions in western Inner Mongolia, China. *Geol. Soc. Am. Bull.* 131(5–6), 941–965. DOI: 10.1130/B32023.1

Liu, X., Chen, B., Jahn, B. M., Wu, G., Liu, Y., 2011. Early paleozoic (ca. 465 ma) eclogites from Beishan (NW China) and their bearing on the tectonic evolution of the southern Central Asian Orogenic Belt. *J. Asian Earth Sci. 42*(4), 715-731. DOI: 10.1016/j.jseaes.2010.10.017

Loury, C., Rolland, Y., Guillot, S., Lanari, P., Ganino, C., Melis, R., Jordon, A., Petit, C., Beyssac, O., Gallet, S., Monié, P. (2018a). Tectonometamorphic evolution of the Atbashi high-P units (Kyrgyz CAOB, Tien Shan): Implications for the closure of the Turkestan Ocean and continental subduction–exhumation of the South Kazakh continental margin. *J. Metamor. Geol.* 36(8), 959-985. DOI: 10.1111/jmg.12423

Loury, C., Rolland, Y., Lanari, P., Guillot, S., Bosch, D., Ganino, C., Jourdon, A., Petit, C., Gallet, S., Monié, P., Riel, N., 2018b. Permian charnockites in the Pobeda area: Implications for Tarim mantle plume activity and HT metamorphism in the South Tien Shan range. *Lithos* 304, 135-154. DOI: 10.1016/j.lithos.2018.01.025

Loury, C., Rolland, Y., Guillot, S., Mikolaichuk, A. V., Lanari, P., Bruguier, O., Bosch, D., 2017. Crustal-scale structure of South Tien Shan: implications for subduction polarity and Cenozoic reactivation, *Geol. Soc. London,* 427, 197-229. DOI: 10.1144/SP427.4

Ma, X. H., Yang, Z. Y., Xing, L. S., Xu, S. J., Zhang, J. X., 1992. A preliminary study on the characteristics of the Permian-Triassic magnetostratigraphy in Ordos Basin. *Chinese Sci. Bull*. 37, 252–255 (in Chinese). DOI: CNKI:SUN:KXTB.0.1992-03-017

Mao, Q. G., Xiao, W. J., Windley, B.F., Han, C.M., Guo, Q.Q., 2012. The Liuyuan complex in the Beishan, NW China: a Carboniferous–Permian forearc sliver in the Southern Altaids. *Geol. Mag.* 149 (3), 483–506. DOI: 10.1017/S0016756811000811

McFadden, P. L., McElhinny, M. W., 1990. Classification of the reversal test in paleomagnetism. *Geophys. J. Int.* 103(3), 725–729. DOI: 10.1111/j.1365-246X.1990.tb05683.x

Mei, H., Yu, H., Li, Q., Lu, S., Li, H., Zuo, Y., Zuo, G., Ye, D, Liu, J., 1999. The first discovery of eclogite and palaeoproterozoic granitoids in the Beishan area, northwestern Gansu Province, China. *Chinese Sci. Bull.* 44, 356–361. DOI: 10.1007/BF02885491

Nie, S. Y., Rowley, D. B., Van der Voo, R., Li, M. S., 1993. Paleomagnetism of late Paleozoic rocks in the Tianshan, northwestern China. *Tectonics*, 12, 568–579. DOI: 10.1029/92TC00657

Niu, Y. Z., Shi, G. R., Wang, J. Q., Liu, C. Y., Zhou, J. L. Lu, J. C., Song, B., Xu, W., 2020. The closing of the southern branch of the Paleo-Asian Ocean: Constraints from sedimentary records in the southern Beishan Region of the Central Asian Orogenic Belt, NW China. *Mar. Petrol. Geol.* 124. DOI: 10.1016/j.marpetgeo.2020.104791

Opdyke, N. D., Channell, J. E. T., 1996. Magnetic stratigraphy. *Int. Geophys. Ser.* 64, 1–346.

Pruner, P., 1992. Palaeomagnetism and palaeogeography of Mongolia from the Carboniferous to the Cretaceous-final report. *Phys. Earth Planet. In.* 70(3-4), 169–177. DOI: 10.1016/0031-9201(92)90179-Y

Ren, Q., Zhang, S., Gao, Y., Zhao, H., Wu, H., Yang, T., Li, H., 2020. New Middle–Late Permian paleomagnetic and geochronological results from Inner Mongolia and their paleogeographic implications. *J. Geophys. Res.* 125, e2019JB019114. DOI: 10.1029/2019JB019114

Renne, P., Swisher, C., Deino, A., Karner, D., Owens, T., DePaolo, D., 1998. Intercalibration of standards, absolute ages and uncertainties in $^{40}Ar/^{39}Ar$ dating. *Chem. Geol.* 145, 117–152. DOI: 10.1016/S0009-2541(97)00159-9

Rolland, Y., Alexeiev, D. V., Kröner, A., Corsini, M., Loury, C., Monié, P., 2013. Late Palaeozoic to Mesozoic kinematic history of the Talas–Ferghana strike-slip fault (Kyrgyz West Tianshan) as revealed by $^{40}Ar/^{39}Ar$ dating of syn-kinematic white mica. *J. Asian Earth Sci.* 67, 76-92. DOI: 10.1016/j.jseaes.2013.02.012

Rolland, Y., Jourdon, A., Petit, C., Bellahsen, N., Loury, C., Sobel, E. R., Glodny, J., 2020. Thermochronology of the highest central Asian massifs (Khan Tengri-Pobedi, SE Kyrgyztan): Evidence for Late Miocene (ca. 8 Ma) reactivation of Permian faults and insights into building the Tian Shan. *J. Asian Earth Sci.* 200, 104466. DOI: 10.1016/j.jseaes.2020.104466

Scaillet S., 2000. Numerical error analysis in $^{40}Ar/^{39}Ar$ dating. *Chem. Geol.* 162: 269-298. DOI: 10.1016/S0009-2541(99)00149-7

Sengör, A. M. C., Natal'in, B. A., Burtman, V. S., 1993. Evolution of the Altaid tectonic collage and Palaeozoic crustal growth in Eurasia. *Nature*, *364*(6435), 299–307. DOI: 10.1038/364299a0

Sharps, R., Li, Y. P., McWilliams, M., Li, Y. G., 1992. Paleomagnetic investigation of upper Permian sediments in the south Junggar Basin, China. *J. Geophys. Res.* 97(B2), 1753–1765. DOI: 10.1029/91JB02741

Sharps, R., Mcwilliams, M., Li, Y., Cox, A., Zhang, Z., Zhai, Y., Gao, Z., Li, Y., Li, Q., 1989. Lower Permian paleomagnetism of the Tarim block, northwestern China. *Earth Planet. Sci. Lett.* 92(3–4), 275–291. DOI: 10.1016/0012-821X(89)90052-6

Shen, S. Z., Shi, G. R., 2002. Paleobiogeographical extinction patterns of Permian brachiopods in the Asian–western Pacific region. *Paleobiology*, 28(4), 449–463. DOI: 10.1666/0094-8373(2002)028<0449:PEPOPB>2.0.CO;2

Simonov, V. A., Sakiev, K. S., Volkova, N. I., Stupakov, S. I., Travin, A. V., 2008. Conditions of formation of the Atbashi Ridge eclogites (South Tien Shan). *Russ. Geol. Geophys.*, 49, 803–815. DOI: 10.1016/j.rgg.2008.04.001

Song, D.F., Xiao, W.J., Windley, B.F., Mao, Q.G., Ao, S.J., Wang, H.Y.C., Li, R., 2021. Closure of the Paleo-Asian Ocean in the Middle-Late Triassic (Ladinian-Carnian): Evidence from provenance analysis of retroarc sediments. *Geophys. Res. Lett.* 48, e2021GL094276. DOI: 10.1029/2021GL094276

Su, B. X., Qin, K. Z., Sun, H., Wang, H., 2010. Geochronological, petrological, mineralogical and geochemical studies of the Xuanwoling mafic–ultramafic intrusion in the Beishan area,

Xinjiang. *Acta Petrol. Sin.* 26, 3283–3294 (in Chinese with English abstract). DOI: CNKI:SUN:YSXB.0.2010-11-011

Su, B. X., Qin, K. Z., Santosh, M., Sun, H., Tang, D. M., 2013. The Early Permian mafic-ultramafic complexes in the Beishan Terrane, NW china: Alaskan-type intrusives or rift cumulates? *J. Asian Earth Sci.* 66, 175-187. DOI: 10.1016/j.jseaes.2012.12.039

Thébault, E., Finlay, C. C., Beggan, C. D., Alken, P., Aubert, J., & Barrois, O., et al., 2015. International Geomagnetic Reference Field: the 12th generation. *Earth Planet Sp.* 67(1), 79. DOI: 10.1186/s40623-015-0228-9

Tian, S., Li, Z., Zhang, Y., Gong, Y., Zhai, D., Wang, M., 2016. Late Carboniferous-Permian tectono-geographical conditions and development in eastern Inner Mengolia and adjacent areas. *Acta Geol. Sin.* 90(4), 688–707. DOI: CNKI:SUN:DZXE.0.2016-04-007

Tian, Z. H., Xiao, W. J., 2020. An Andean-type arc transferred into a Japanese-type arc at final closure stage of the Palaeo-Asian Ocean in the southernmost of Altaids. *Geol. J.* 55(3), 2023-2043. DOI: 10.1002/gj.3700

Wang, B., Chen, Y., Zhan, S., Shu, L., Faure, M., Cluzel, D., Laurent-Charvet, S., 2007. Primary Carboniferous and Permian paleomagnetic results from the Yili Block (NW China) and their implications on the geodynamic evolution of Chinese Tianshan Belt. *Earth Planet. Sci. Lett.* 263(3-4), 288–308. DOI: 10.1016/j.epsl.2007.08.037

Wang, B., Cluzel, D., Jahn, B. M., Shu, L., Chen, Y., Zhai, Y., Branquet, Y., Barbanson, L., Sizaret, S., 2014. Late Paleozoic pre- and syn-kinematic plutons of the Kangguer-Huangshan shear zone; inference on the tectonic evolution of the eastern Chinese north Tianshan. *Am. J. Sci.* 314(1), 43–79. DOI:10.2475/01.2014.02

Wang, B., Cluzel, D., Shu, L., Faure, M., Charvet, J., Chen, Y., Meffre, S., de Jong, K., 2009. Evolution of calc‐alkaline to alkaline magmatism through carboniferous convergence to Permian transcurrent tectonics, western Chinese Tianshan. *Int. J. Earth Sci.* 98(6), 1275–1298. DOI: 10.1007/s00531‐008‐0408‐y

Wang, B., Song, F., Ni, X. H., Cao, T. T., Liu, J. S., Zhong, L. L., Sun, Z. C., Sun, Y. X., Deng, J., Li, Y. Y., Zhu, X., Liu, H. S., He, Z. Y., 2022. Paleozoic accretionary orogenesis and major transitional tectonic events of the Tianshan orogen. *Acta Geol. Sin.* 96(10), 3514-3540 (in Chinese with English abstract). DOI: 10.19762/j.cnki.dizhixuebao.2022081

Wang, B., Zhai, Y. Z., Kapp, P., de Jong, K., Zhong, L. L., Liu, H. S., Ma, Y. Z., Gong, H. J., Geng, H. Y., 2018. Accretionary tectonics of back-arc oceanic basins in the South Tianshan: insights from structural, geochronological, and geochemical studies of the Wuwamen ophiolite melange. *Geol. Soc. Am. Bull.* 130, 284–306. DOI: 10. 1130/b31397.1

Wang, Y., Luo, Z. H., Santosh, M., Wang, S. Z., Wang, N., 2016. The Liuyuan Volcanic Belt in NW China revisited: evidence for Permian rifting associated with the assembly of continental blocks in the Central Asian Orogenic Belt. *Geol. Mag.* 154(02), 265-285. DOI: 10.1017/S0016756815001077

Webb, L. E., Johnson, C. L., Minjin, C., 2010. Late Triassic sinistral shear in the East Gobi Fault Zone, Mongolia. *Tectonophysics* 495, 246–255. DOI: 10.1016/j.tecto.2010.09.033

Wei, B., Yang, X., Cheng, X., Domeier, M., Wu, H., Kravchinsky, V. A., Zhou, Y., Jiang, N., Wu, Y., Huo, F., Zhang, W., Zhang, Y., Shao, R., 2020. An absolute paleogeographic positioning of the early Permian Tarim large igneous province. *J. Geophys. Res.* 125(5), e2019JB019111. DOI: 10.1029/2019JB019111

Wu, H. N., Zhou, L. F., Zhao, Z. Y., 1993. Paleomagnetic study of Carboniferous and Permian rocks from the Alashan and surrounding regions and its tectonic implications. *Sci. China Ser. B* 23(5), 527–536. (in Chinese). DOI: CNKI:SUN:JBXK.0.1993-05-011

Xiao, W. J., Mao, Q., Windley, B. F., Han, C. M., Qu, J. F., Zhang, J. E., Ao, S. J., Guo, Q. Q., Cleven, N. R., Lin, S. F., 2010. Paleozoic multiple accretionary and collisional processes of the Beishan orogenic collage. *Am. J. Sci.* 310, 1553–1594. DOI: 10.2475/10.2010.12

Xiao, W. J., Windley, B. F., Hao, J., Zhai, M. G., 2003. Accretion leading to collision and the Permian Solonker suture, Inner Mongolia, China: termination of the central Asian orogenic belt. *Tectonics*, 22(6), 1069. DOI: 10.1029/2002TC001484

Xiao, W. J., Windley, B. F., Sun, S., Li, J. L., Huang, B. C., Han, C. M., Yuan, C., Sun, M., Chen, H. L., 2015. A tale of amalgamation of three Permo-Triassic Collage Systems in Central Asia: Oroclines, sutures, and terminal accretion. *Annu. Rev. Earth Planet. Sci. 43*(1), 477–507. DOI: 10.1146/annurev-earth-060614-105254

Xu, B., Charvet, J., Chen, Y., Zhao, P., Shi, G. Z., 2013. Middle Paleozoic convergent orogenic belts in western Inner Mongolia (China): Framework, kinematics, geochronology and implications for tectonic evolution of the Central Asian Orogenic Belt. *Gondwana Res.* 23(4), 1324–1364. DOI:10.1016/j.gr.2012.05.015

Xu, G., Duan, J., Gao, W. B., Wang, R. M., Shi, Z., Ma, B. C., Sun, J., 2021. Geochronological and Geochemical Constraints on the Petrogenesis of Permian Dolerite Dyke Swarms in the Beishan Orogenic Belt, NW China. *Front. Earth Sci.* 9, 657716. DOI: 10.3389/feart.2021.657716

Xu, W., Sun, Z. M., Shi, G. R., Lu, J. C., Yu, L., Niu, Y. Z., Zhao, Y., Han, X. F., Wang, B. W., Song, B., Cao, Y., 2019. First report of coupled Early Permian paleomagnetic and geochronologic data from the Dunhuang block (NW China), and its implications for the tectonic evolution of the Paleo-Asian ocean. *Gondwana Res.* 67, 46-63. DOI: 10.1016/j.gr.2018.10.012

Xu, X., Harbert, W., Dril, S., Kravchinksy, V., 1997. New paleomagnetic data from the Mongol–Okhotsk collision zone, Chita region, south-central Russia: Implications for Paleozoic paleogeography of the Mongol–Okhotsk Ocean. *Tectonophysics* 269(1-2), 113–129. DOI: 10.1016/S0040-1951(96)00140-0

Yuan, W., Yang, Z. Y., 2015a. The Alashan Terrane was not part of North China by the Late Permian: Evidence from Carboniferous and Permian paleomagnetic results. *J. Asian Earth Sci.* 104, 145-159. DOI: 10.1016/j.jseaes.2014.02.010

Yuan, W., Yang, Z. Y., 2015b. The Alashan Terrane was not part of North China by the Late Devonian: Evidence from detrital zircon U-Pb geochronology and Hf isotopes. *Gondwana Res.* 27(3), 1270-1282. DOI: 10.1016/j.gr.2013.12.009

Yuan, Y., Zong, K., He, Z., Klemd, R., Liu, Y., Hu, Z., Guo, J., Zhang, Z., 2015. Geochemical and geochronological evidence for a former early Neoproterozoic microcontinent in the south Beishan Orogenic Belt, southernmost Central Asian Orogenic Belt. *Precambrian Res.* 266, 409-424. DOI: 10.1016/j.precamres.2015.05.034

Zhang, D. H., Huang, B. C., Zhao, J., Meert, J. G., Zhang, Y., Liang, Y. L., Bai, Q. H., Zhou, T. H., 2018. Permian paleogeography of the eastern CAOB: Paleomagnetic constraints from volcanic rocks in central eastern Inner Mongolia, NE China. *J. Geophys. Res.* 123(4), 2559–2582. DOI: 10.1002/2018JB015614

Zhang, D. H., Huang, B. C., Zhao, G. C., Meert, J. G., Williams, S., Zhao, J., Zhou, T. H, 2021a. Quantifying the extent of the Paleo-Asian Ocean during the Late Carboniferous to Early Permian. *Geophys. Res. Lett.* 48, e2021GL094498. DOI: 10.1029/2021GL094498

Zhang, D. H, Huang, B. C, Meert, J. G., Zhao, G. C, Zhao, J., Zhao, Q, 2021b. Micro-blocks in NE Asia amalgamated into the unified Amuria block by ~300 Ma: First paleomagnetic evidence from the Songliao block, NE China. *J. Geophys. Res.* 126, e2021JB022881. DOI: 10.1029/2021JB022881

Zhang, L.F., Ai, Y.L., Li, X.P., Rubatto, D., Song, B., Williams, S., Song, S.G., Ellis, D., Liou, J.G., 2007. Triassic collision of western Tianshan orogenic belt, China: evidence from SHRIMP U-Pb dating of zircon from HP/UHP eclogitic rocks. *Lithos* 96, 266–280. DOI: 10.1016/j.lithos.2006.09.012

Zhang, W., Wu, T. R., He, Y. K., Feng, J. C., Zheng, R. G., 2010. LA-ICP-MS zircon U–Pb ages of Xijianquanzi alkali-rich potassium-high granites in Beishan, Gansu Province, and their tectonic significances. *Acta Petrol. Miner.* 29, 719–731 (in Chinese with English abstract). DOI: 10.3969/j.issn.1000-6524.2010.06.009

Zhang, W., Wu, T., Zheng, R., Feng, J., Luo, H., He, Y., Cao, X., 2012. Post-collisional Southeastern Beishan granites: Geochemistry, geochronology, Sr-Nd-Hf isotopes and their implications for tectonic evolution. *J. Asian Earth Sci. 58*, 51-63. DOI:

10.1016/j.jseaes.2012.07.004

Zhang, Y., Muxworthy, A. R., Jia, D., Wei, G., Xia, B., Wen, B., Wang, M., Liu, W., Brzozowski, M., 2019. Identifying and dating the destruction of hydrocarbon reservoirs using secondary chemical remanent magnetization. *Geophys. Res. Lett.* 46(20), 11100-11108. DOI: 10.1029/2019GL084812

Zhang, Y., Yuan, C., Sun, M., Long, X., Xia, X., Wang, X., Huang, Z., 2015. Permian doleritic dikes in the Beishan Orogenic Belt, NW China: Asthenosphere-lithosphere interaction in response to slab break-off. *Lithos*, 233(4), 174-192. DOI: 10.1016/j.lithos.2015.04.001

Zhao, G. C, Wang, Y. J, Huang, B. C, Dong, Y. P, Yu, S., 2018. Geological reconstructions of the East Asian blocks: from the breakup of Rodinia to the assembly of Pangea. *Earth Sci. Rev.* 186, 262-286. DOI: 10.1016/j.earscirev.2018.10.003

Zhao, P., Appel, E., Xu, B., Sukhbaatar, T., 2020. First paleomagnetic result from the Early Permian volcanic rocks in northeastern Mongolia: Evolutional implication for the Paleo-Asian Ocean and the Mongol-Okhotsk Ocean. *J. Geophys. Res.* 125, e2019JB017338. DOI: 10.1029/2019JB017338

Zhao, P., Chen, Y., Xu, B., Faure, M., Shi, G., Choulet, F., 2013. Did the Paleo-Asian Ocean between North China Block and Mongolia Block exist during the late Paleozoic? First paleomagnetic evidence from central-eastern Inner Mongolia, China. *J. Geophys. Res.* 118(5), 1873–1894. DOI: 10.1002/jgrb.50198

Zhao, X., Coe, R. S., Zhou, Y., Wu, H., Wang, J., 1990. New paleomagnetic results from northern China: Collision and suturing with Siberia and Kazakhstan. *Tectonophysics* 181(1-4), 43–81. DOI: 10.1016/0040-1951(90)90008-V

Zhu, X., Wang, B., Chen, Y., Liu, H., 2019. Constraining the Intracontinental Tectonics of the SW Central Asian Orogenic Belt by the Early Permian Paleomagnetic Pole for the Turfan-Hami Block. *J. Geophys. Res.* 124(12), 12366-12387. DOI: 10.1029/2019JB017680

Zhu, X., Wang, B., Chen, Y., Liu, H., Horng, C. S. Choulet, F., Faure, M., Shu, L., Xue, Z., 2018. First early Permian paleomagnetic pole for the Yili block and its implications for late Paleozoic postorogenic kinematic evolution of the SW central Asian Orogenic Belt. *Tectonics*, 37(6), 1709–1732. DOI: 10.1029/2017TC004642

Zijderveld, J. D. A., 1967. A.C. demagnetization of rocks: Analysis of results. In D. W. Collinson, K. M. Creer, & S. K. Runcorn (Eds.), Methods on Paleomagnetism (pp. 245–286). New York: Elsevier.

Figure captions

Figure 1. (a) Simplified tectonic division of eastern Asia (after Jahn, 2004). EEC: East European Craton; KZN: Kazakhstan; Q: Qaidam; SLF: Solonker Fault; STS: South Tianshan Suture; (b) geologic map of the Beishan region showing the location of the sampling area (after Xiao et al., 2010 & He et al., 2018a); (c) satellite image of studied Gubaoquan doleritic dikes (the yellow dashed lines).

Figure 2. (a, b) Panorama photo and a sketch of the studied doleritic dike swarm (black) intruding orthogneisses (white) in the Gubaoquan area; (c) baked contact between a doleritic dike and orthogneissic country rock; (d) partial enlarged picture showing vertical to sub-vertical doleritic dikes; (e) augen structure of the country rock.

Figure 3. (a-c) Thermomagnetic curves and (d-g) hysteresis loops of representative samples; (h) Day plot of hysteresis parameters of 16 representative samples; (i) plot of anisotropy degree (P_J) versus anisotropy shape (T) of magnetic susceptibility of samples collected from doleritic dikes (in black) and country rocks (orthogneisses, in blue); (j-k) anisotropy of magnetic susceptibility measurement results of doleritic dikes (in black) and their country rocks (in blue), respectively.

Figure 4. Scanning electronic microscope observations and representative energy-dispersive X-ray spectrometer results: (a-c) irregular magnetite grains without evident alteration showing exsolution; (d) Ti-poor Magnetite grains with the appearance of alteration probably due to excessive polishing; (e-f) irregular pyrite (Py), chalcopyrite (Cp), and ilmenite (Ilm) grains; (g-h) iron oxide rims of pyrite grains; and (h-i) cracks and pores without authigenic magnetic minerals.

Figure 5. (a-b) Representative microphotographs of Sample BS30-32 (Cpx, clinopyroxene; Pl, plagioclase; Hbl, hornblende; Oxd, Fe-Ti oxides); (c) $^{40}Ar/^{39}Ar$ geochronologic results of plagioclases extracted from Sample BS30-32. WMA refers to the weighted mean age.

Figure 6. Representative demagnetization curves in the geographic coordinates for specimens from (a-b & d-i) the doleritic dikes and (j-k) the orthogneisses. Note: blue arrow represents low unblocking temperature or low-coercivity component (LTC or LCC), and red arrow represents characteristic remanent magnetization (ChRM); (c) equal-area projection of isolated LTCs and LCCs, and the comparison between their mean-direction (red star) and present earth field (grey diamond).

Figure 7. Equal-area projections in the geographic coordinates of (a-b) dike-mean directions and specimens' ChRM directions of Group A and their Fisher mean

directions (red and blue pentagrams, respectively); (c) specimens' ChRM directions of Group B and the Fisher mean direction.

Figure 8. (a) Directional independence evaluation of the dike-mean directions from the Group A; (b) equal-area projection of 8 virtual geomagnetic poles (VGPs) calculated from independent direction groups and their Fisher mean (red pentagram); (c) the comparison between the mean directions on specimen-level of Group A (in black) and Group B (in red).

Figure 9. (a) The compilation of Early Permian paleomagnetic poles for major blocks in the southern CAOB (details in Text S1 and Table S2). (b) Early Permian paleogeographic reconstruction of south CAOB (achieved using Gplates). The color of the paleopole matches the color of the corresponding block. Fixed plate ID: 000 (Earth's spin axis). Euler rotation parameters: Tarim (-4.7°, 95.2°, 30.3°), Junggar (-67.2°, -120.9°, 52.9°), Yili (-64.9°, 152.9°, 27.2°), Turpan-Hami (-70.1°, 169.2°, 28.6°), Beishan (-66.2°, -161.4°, 26.8°), Dunhuang (-59.1°, 158.2°, 24.0°), Mongolia (-49.3°, -110.1°, 58.5°), and North China (-47.9°, -112.7°, 59.3°). The longitude of the Tarim block is assigned according to its absolute reconstruction introduced in Wei et al. (2020). The paleo-position of the Qaidam-Central Qilian Block is without constraint from paleomagnetic data. The Early Permian paleogeographic configuration of other East Asian blocks is mainly modified after Dong et al. (2021).

Author agreement

Dear Editor,

We there undersigned declare that this manuscript entitled '*Paleomagnetic study on the Early Permian Gubaoquan doleritic dike swarm in the southern Beishan area, NW China: Implications for the tectonic and paleogeographic reconstructions of the southern Central Asian Orogenic Belt*' is original, has not been published before and is not currently being considered for publication elsewhere.

We confirm that the manuscript has been read and approved by all named authors and that there are no other persons who satisfied the criteria for authorship but are not listed. We further confirm that the order of authors listed in the manuscript has been approved by all of us. We understand that the Corresponding Author is the sole contact for the Editorial process. He is responsible for communicating with the other authors about progress, submissions of revisions and final approval of proofs.

Signed by all author as follows:

Xin Zhu

Yan Chen

Bo Wang (corresponding author)

Yunpeng Dong

Stéphane Scaillet

Michel Faure

Xinghua Ni

Florian Duval

Xin Zhu: Conceptualization, Investigation, Writing - Original draft; **Yan Chen**: Methodology, Writing - Review & Editing, **Bo Wang**: Funding acquisition, Writing - Review & Editing; **Yunpeng Dong**: Writing - Review & Editing; **Stéphane Scaillet**: Investigation, Formal analysis; **Michel Faure**: Investigation; Writing - Review & Editing; **Xinghua Ni**: Investigation; **Florian Duval**: Investigation.

Declaration of interests

☑The authors declare that they have no known competing financial interests or personal relationships that could have appeared to influence the work reported in this paper.

☐The authors declare the following financial interests/personal relationships which may be considered as potential competing interests:

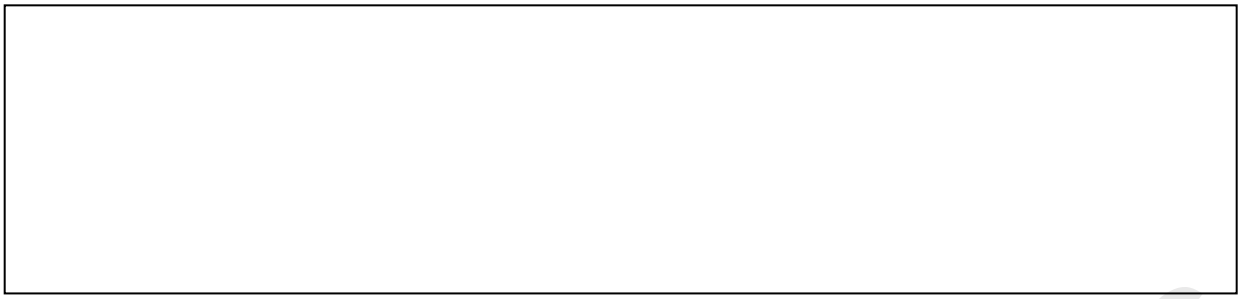

- The Gubaoquan doleritic dike swarm intruded at ~282-286 Ma
- The Early Permian paleomagnetic pole for the Beishan region is obtained
- No broad ocean existed between Beishan and Dunhuang in the Early Permian
- The southern CAOB presented a WNW-ESE distributed paleogeography in the Early Permian

Table 1. Paleomagnetic results of the doleritic and orthogneissic specimens collected from the Gubaoquan area, Beishan region.

Site	S-Lat (N)	S-Long (E)	n/n_o (**N**)	R/N	D_g (°)	I_g (°)	k	α_{95} (°)	P-Lat (N°)	P-Long (E°)	A_{95} (°)
Group A											

DD01	40°59′20.679″	95°02′9.964″	5/6	5/0	196.9	-48.7	1644.8	1.9	72.2	219.3	2.0
DD05			5/6	5/0	170.7	-58.4	523.9	3.3	82.6	353.1	4.2
DD06	40°59′21.893″	95°02′5.441″	5/6	5/0	161.6	-46.5	90.0	8.1	69.9	329.5	8.3
DD09			11/12	11/0	188.6	-56.1	354.8	2.4	82.0	215.2	3.0
DD10			6/6	6/0	188.6	-54.4	1270.4	1.9	80.9	224.1	2.3
DDs 0910			*17/18*	*17/0*	*188.6*	*-55.5*	*474.8*	*1.6*	*81.6*	*218.7*	*1.9*
DD11			6/7	6/0	194.7	-64.6	534.6	2.9	78.1	152.7	4.2
DD12			0/6								
DD13			5/6	5/0	165.6	-35.9	240.3	4.9	65.6	309.5	4.3

DD14			6/6	6/0	166.7	-40.5	75.9	7.7	68.9	311.0	7.2
DDs 1314			*11/11*	*11/0*	*166.2*	*-38.4*	*256.2*	*4.4*	*67.4*	*310.2*	*4.0*
DD17	40°59′41.243″	95°02′25.908″	13/15	13/0	176.3	-49.9	94.2	4.3	79.3	292.3	4.7
DD19	40°59′37.725″	95°02′24.556″	5/6	5/0	176.8	-54.7	961.3	2.5	83.7	299.6	3.0
Mean[10]			**10**	**10/0**	**177.4**	**-51.6**	**48.3**	**7.0**			
Mean[8]			***8***	***8/0***	***177.9***	***-52.7***	***51.1***	***7.8***	***82.8***	***285.6***	***9.2***
Mean*			***67s/82s***	***21s/0***	***178.3***	***-52.0***	***48.2***	***2.5***			
Group B (qualitative reference dikes)											
DD02			2/2	2/0	176.9	-51.1					
DD03	40°59′20.635″	95°02′9.063″	3/3	3/0	163.3	-43.7	71.2	14.7			

DD04	40°59′21.268″	95°02′8.323″	2/2	2/0	199.2	-48.7		
DD07			2/2	2/0	169.6	-54.1		
DD08			2/2	2/0	159.2	-56.9		
DD15			2/2	2/0	185.6	-53.8		
DD16			3/3	3/0	162.4	-54.7	150.4	10.1
DD18	40°59′38.506″	95°02′25.636″	3/3	3/0	173.7	-55.8	761.8	4.5
DD20	40°59′37.333″	95°02′24.152″	2/2	2/0	187.5	-54.5		
Mean*			***21s/21s***	***21s/0***	***174.0***	***-53.1***	***63.2***	***4.0***
Orthogneissic specimens (country rock)								
OG01	40°59′20.605″	95°02′9.676″	1/1	1/0	163.6	-25.4		

OG02	40°59′21.707″	95°02′7.543″	0/4			
OG03			1/7	1/0	156.7	-30.7
OG04	40°59′25.065″	95°02′1.673″	1/4	1/0	162.6	-43.0

Abbreviations: Slat (N°)/ Slong (N°), latitude and longitude of sampling sites. n/n_0 (**N**), number of specimens (sites) in calculation/studied.

R/N, reversed/normal polarity.

Dg and Ig, declination (D) and inclination (I) in geological (g) coordinates; k, precision parameter; α95, 95% confidence interval.

$Plat_g$, $Plong_g$, and A_{95}, latitude and longitude of paleomagnetic poles in geographic ($_g$) coordinates, and 95% confidence interval.

DD and OG means doleritic dike and orthogneiss, respectively.

Mean[10]: Fisher mean from dike-mean directions of Group A. ***Mean[8]***: Fisher mean from independent direction groups.

Mean*: Fisher mean in specimen-level.

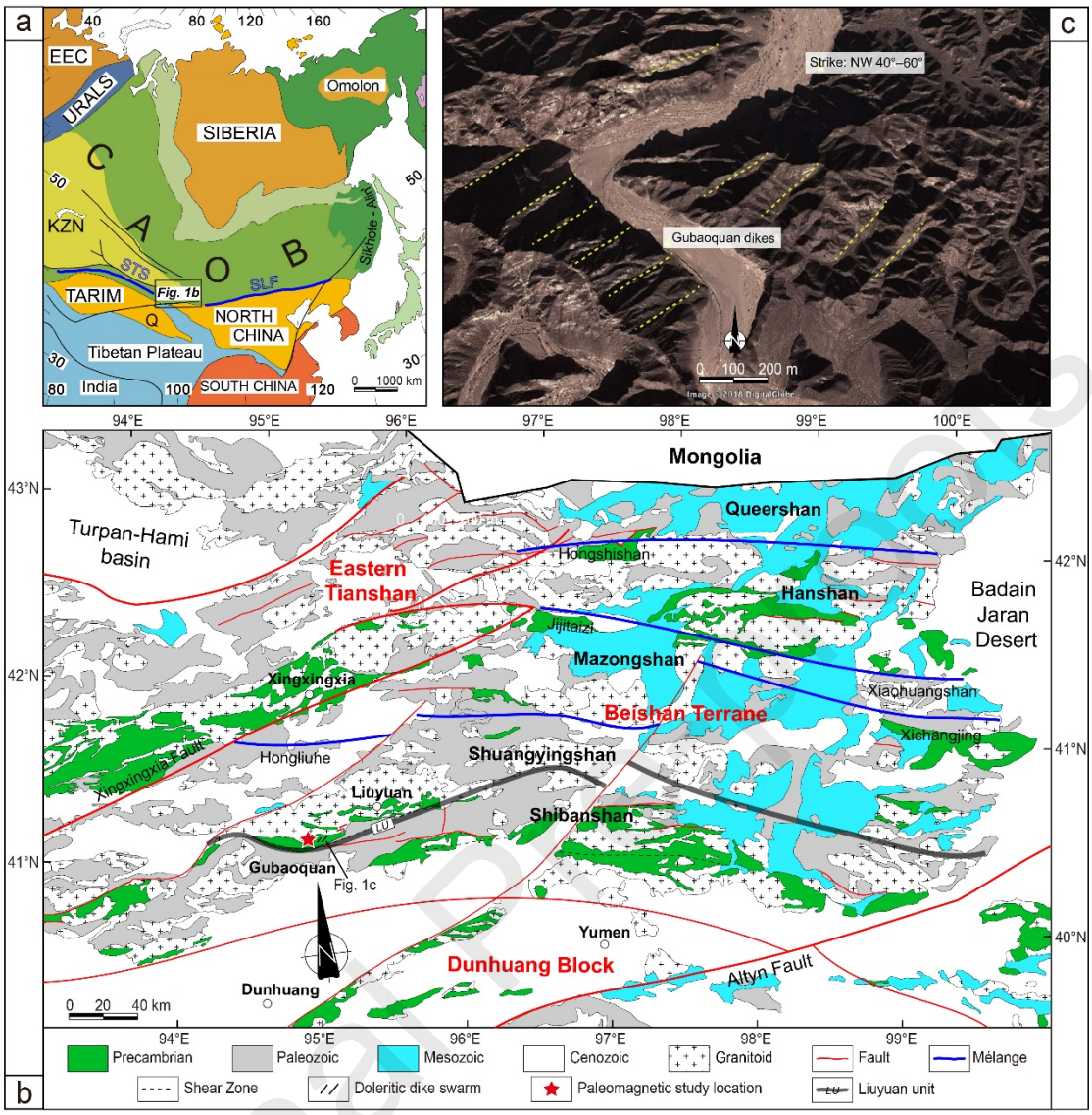

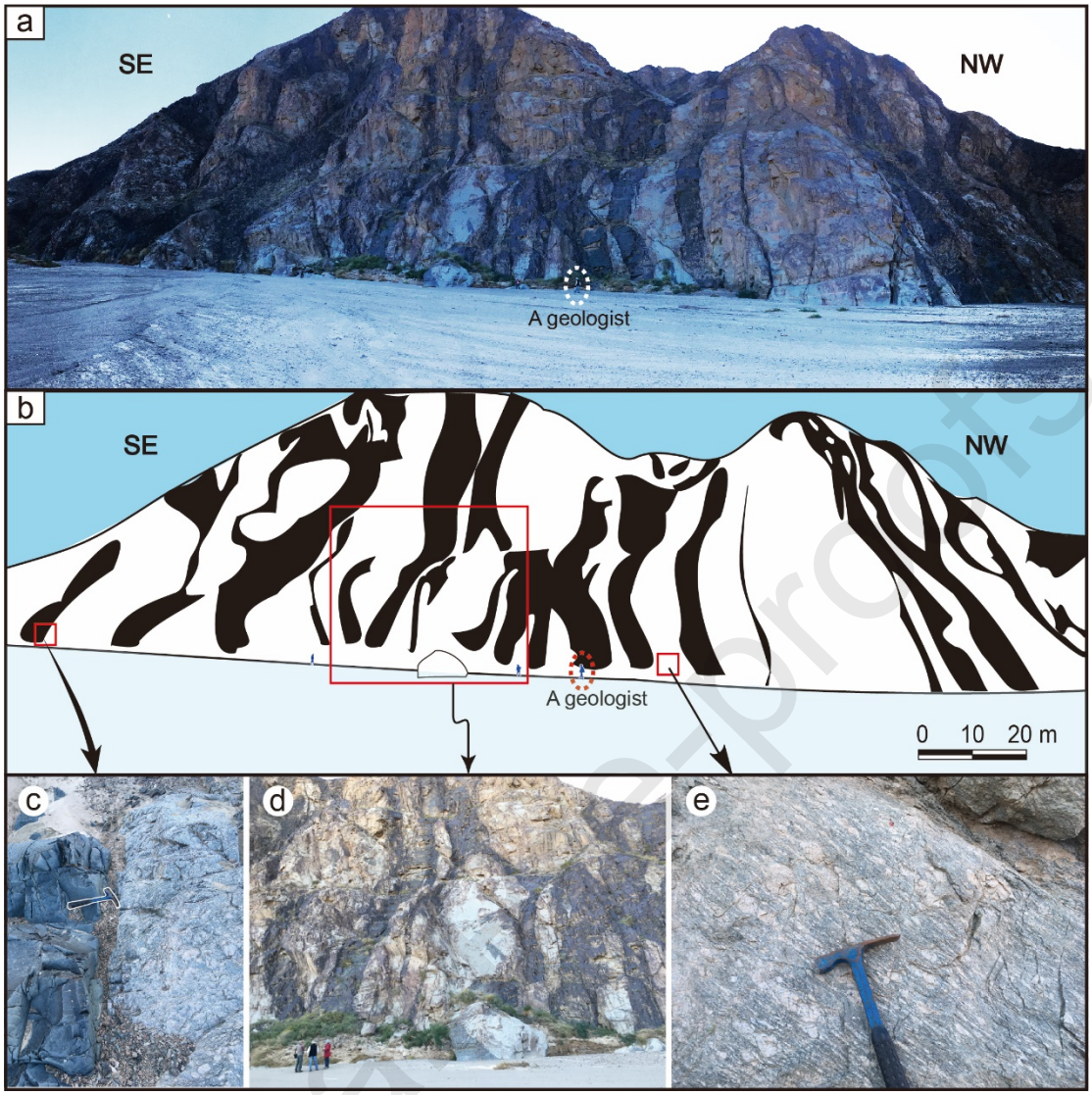

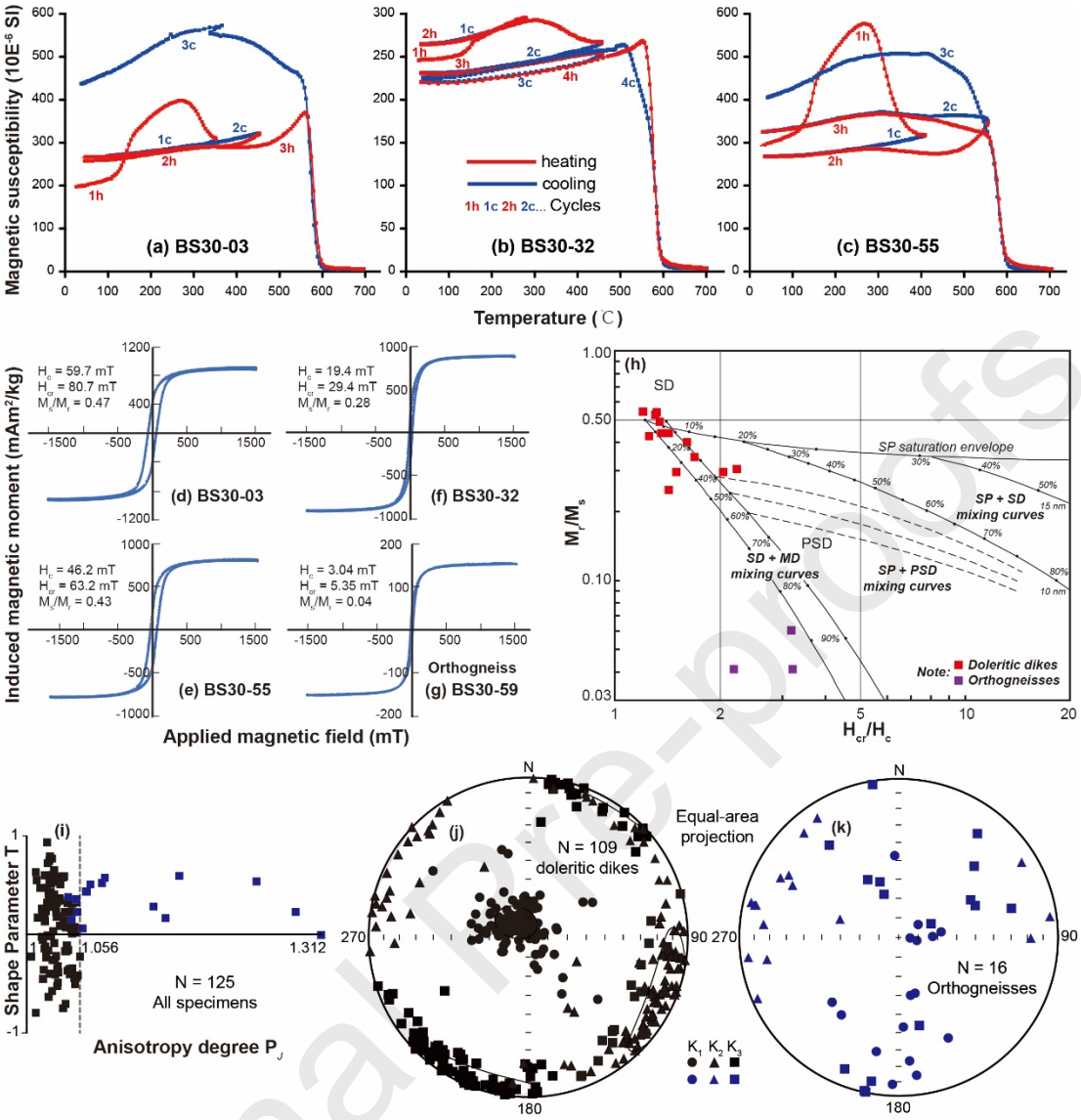

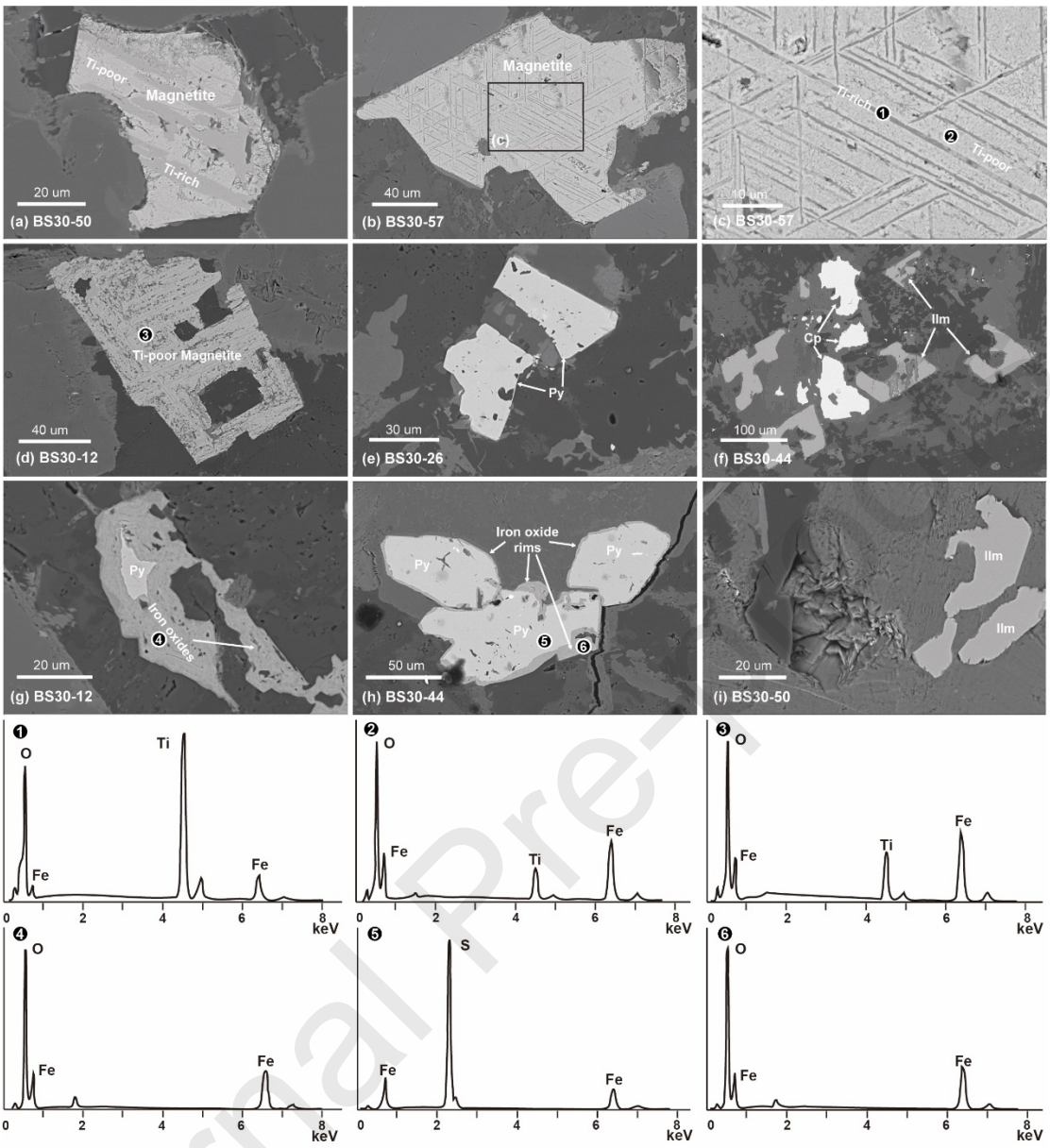

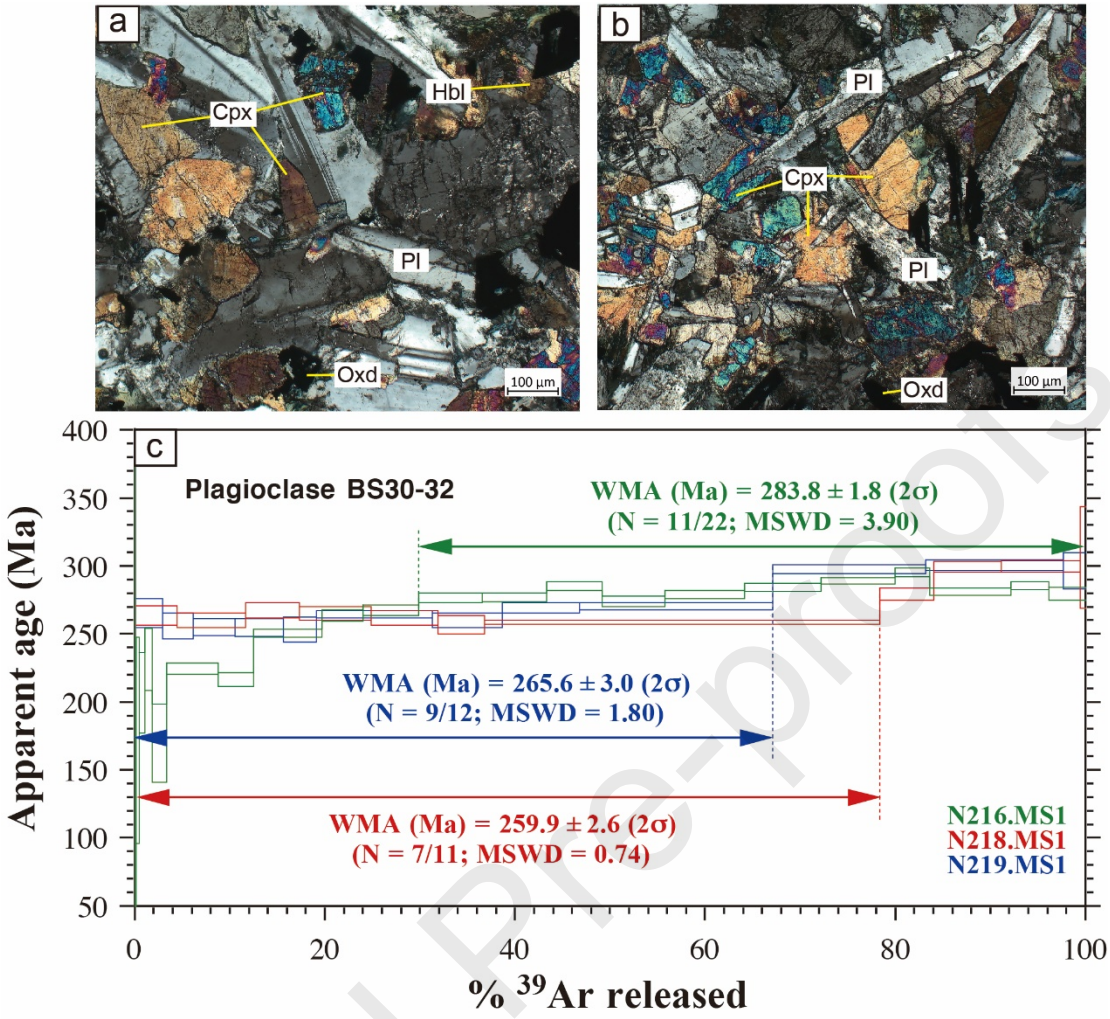

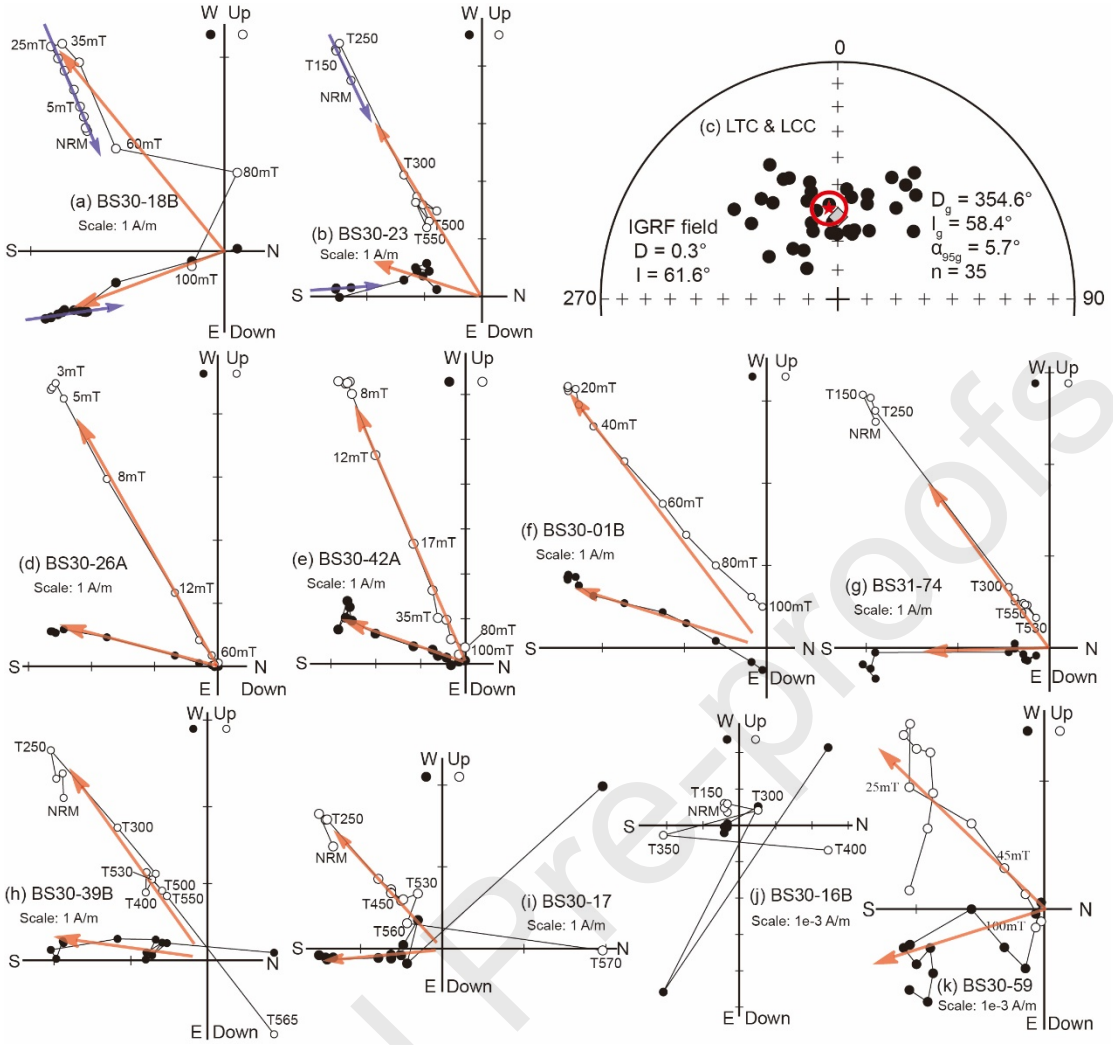

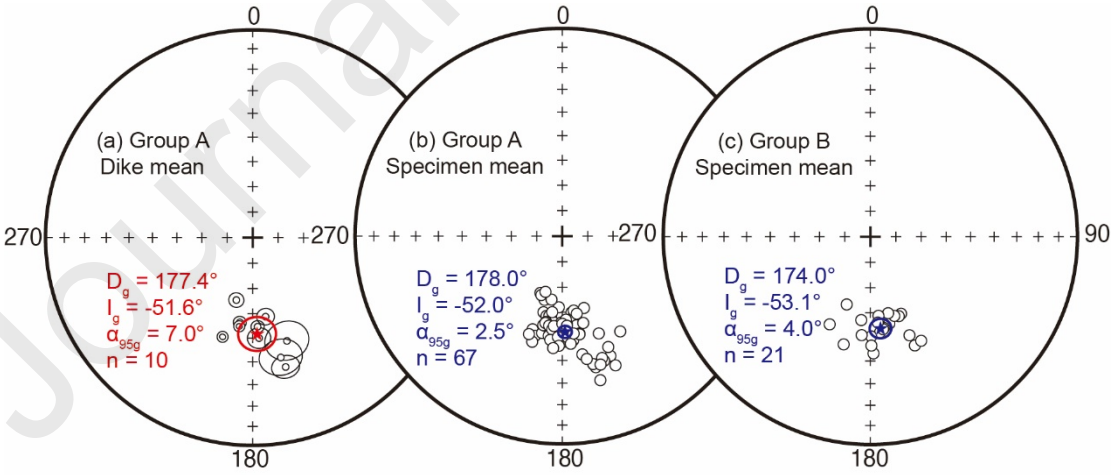

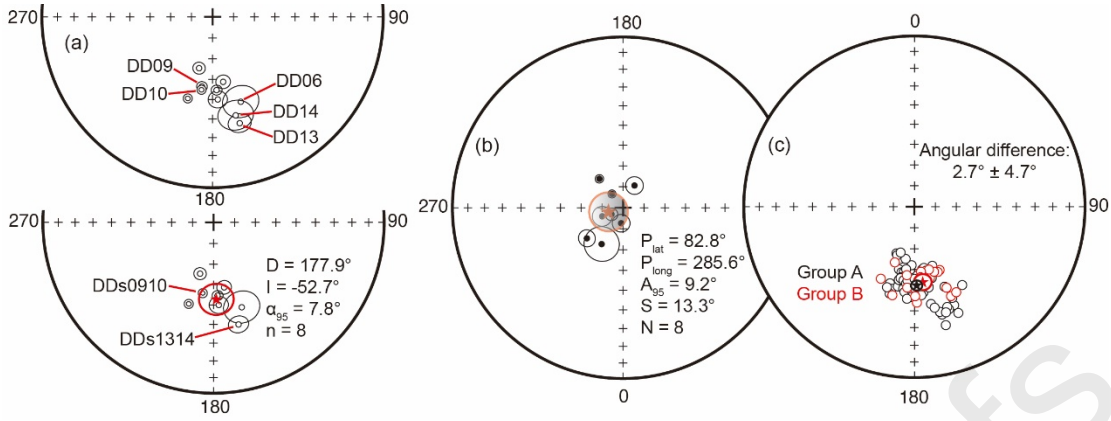

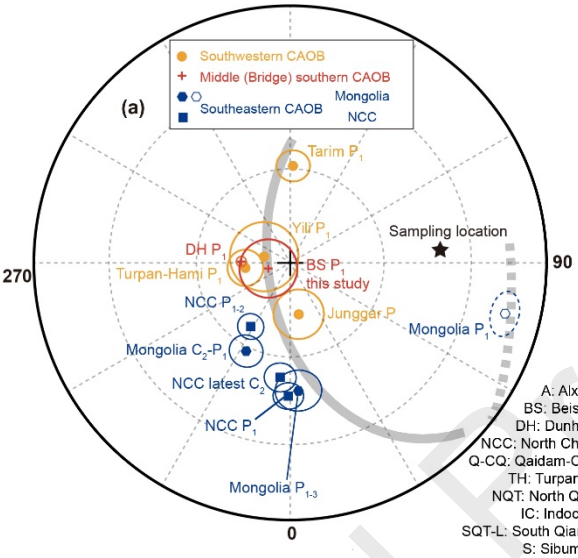

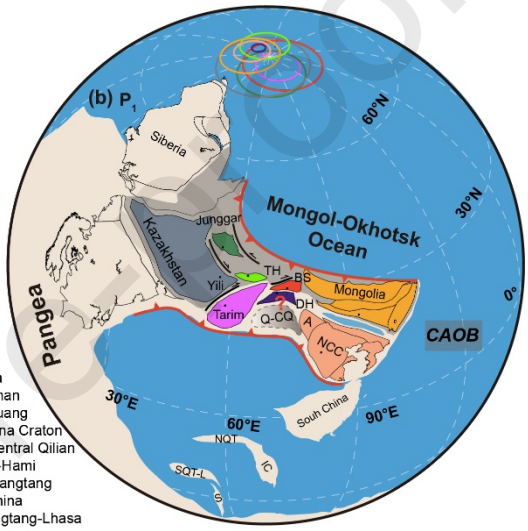

A: Alxa
BS: Beishan
DH: Dunhuang
NCC: North China Craton
Q-CQ: Qaidam-Central Qilian
TH: Turpan-Hami
NQT: North Qiangtang
IC: Indochina
SQT-L: South Qiangtang-Lhasa
S: Sibumasu